Chapter 14

Study of the Murine Cardiac Mechanical Function Using Magnetic Resonance Imaging: The Current Status, Challenges, and Future Perspectives

Christakis Constantinides

Additional information is available at the end of the chapter

http://dx.doi.org/10.5772/51364

1. Introduction

While cardiac mechanical function studies initially focused on large mammals and the human, the mouse emerged as the preferred animal species for such research in recent years [Collins 2003]. Despite the fact that evidence supports that bio-energetically and hemodynamically the mouse scales in a linear fashion with larger mammals and humans [Dobson 1995, Nielsen 1958], nevertheless, important physiological questions still remain [Kass 1998, Balaban 2001] on whether such a model is the most appropriate for extrapolation of conclusions to man [Schaper 1998, Balaban 2012]. With the complete characterization of the mouse and human genomes (a National Institutes of Health initiative) in 2002 and 2003 respectively [Collins 2003, Gregory 2002], a plethora of mouse studies emerged targeting the cardiovascular system in animals with genetic modifications [James 1998, Hoit 2001, Gehmann 2000, Ehmke 2003], marking the onset of the molecular physiology, proteomics, and (structural and functional) genomics era. Collectively, these studies [Milano 1994, Barbee 1994, MacGowan 2001] initially targeted six important areas of cardiac function including the: *(a) excitation-contraction cascade*; *(b) the beta-adrenergic system*; *(c) the cytosolic/structural system and the cytoskeleton*; *(d) the extracellular matrix and its coupling to important cytosolic elements that assist the mechanical force generation or propagation*; *(e) molecules that determine spatial-temporal mechanical changes (due to differential gene expression, phosphorylation, or recruitment of fetal development gene programs)*; and *(f) the energetic-metabolic status of the muscle*. Equally important in most of these studies was the non-invasive imaging of such animals for phenotypic and genotypic screening, often conducted under inhalational anesthesia [Erhart 1984, Hart 2001, Price 1980, Kober 2005, Constantinides_ILAR 2011].

Despite the existence of a plethora of cardiac functional techniques for characterization of mechanical structure, function and dysfunction, a parallel need exists for development of invasive and non-invasive tools and techniques to describe the left ventricular (LV) tissue material properties as these relate to the: (a) mechanical pumping function of the LV; (b) myocardial oxygen demand defining myocyte metabolic status; (c) coronary blood flow and its auto-regulation; (d) arhythmogenic risk; (e) cell-signaling pathways responsible for growth and remodeling during development and disease. Reinforcing basic physiology work, invasive catheterization experiments [Georgakopoulos 1998] have also allowed determination of inotropic and lusitropic cardiac status, while Magnetic Resonance Imaging (MRI) experimentation, methodologies and technology advances have facilitated migration of such work to a non-invasive imaging platform, with tremendous potential for future basic science and translational research.

Specifically, advances in MRI techniques (myocardial spin tagging [Zerhouni 1988, Axel 1989], DENSE [Aletras 1999], and harmonic phase imaging [Osman 1999]) have been introduced over the last decades to quantify cardiac function, allowing myocardial tracking, motion and strain quantification in normal and genetically engineered mice [Rockman 1991, Franco 1999, Brede 2001, Yang 2002, Engel 2004, Wilding 2005]. Critical to such work has been the validation of the underlying hypothesis of morphological and functional scaling from mouse to human (through consideration of global cardiac function, circulatory control, blood flow distribution, Ca^{2+} storage and cycling, myosin light chain distribution, and force frequency reserve), for comparative studies.

This chapter provides an overview of the major physiological issues and challenges for mouse MR imaging and discusses the most recent and major advances in conventional and new cardiac Magnetic Resonance imaging strategies, that ultimately allow quantification of motion, global, and regional cardiac function, strain, and elasticity, characterizing inotropic and lusitropic contractile function and dysfunction in humans and transgenic mice for image-based phenotyping.

Specifically, this chapter attempts a detailed reference to the mouse as a research model, focusing on its genetic background and homology with the human genome and to the developmental and morphological differences between mouse and man, thus addressing cellular and global organ similarities and differences. As a basic determinant of structure, cardiac functional differences are associated, justified by carefully-controlled indices that determine integrative physiological control and functional activities, including metabolism, perfusion, angiogenetic, collateral flow, and coronary reserve. The importance and impact of anesthesia for image-based phenotyping in patho-physiological status is addressed with brief references to the possible mechanisms and cellular and sub-cellular target sites of anesthesia action. The section is complemented with recent findings on heart rate variability (as a result of the widely used inhalational anesthesia use) under optimal anesthesia conditions using isoflurane and long term physiological stability elicited from the use of the balancing anesthetic, Nitrous Oxide.

A historical overview of the evolution of mouse cardiac MRI is also attempted (in direct correlation with the evolution and progress of human clinical cardiac MRI, radiofrequency

(RF), and gradient technologies) based on recent work and advances in miniature RF coils for imaging, state-of-the-art imaging techniques and pulse sequences based on rectilinear and non-cartesian sampling schemes, including functional MRI, atlas-based approaches for morphology assessment and four-dimensional (4D) motional variability, as well as regional cardiac functional characterization and quantification methods, Displacement Encoding with Stimulated Echoes (DENSE) [Aletras 1999], Harmonic Phase (HARP) [Osman 1999, Kuijer 2001], tagging and advanced imaging techniques. MRI-based, accurate three-dimensional (3D) and 4D surface and finite element mesh model extractions, in association with advanced segmentation – seed-based or semi-automatic - and registration techniques – diffeomorphic or landmark-based, are shown to facilitate efficient mouse inter-strain cardiac hemodynamical comparisons of both right and left-ventricular chambers. Based on recently published DENSE human-mouse comparative studies, and findings from image-based regional functional quantifications, similar transmural motional patterns are observed in both species, lending additional support to long-standing hypotheses for the existence of allometric scaling in metabolism, energetics [Dobson 1995, Nielsen 1958, Phillips 2012], and mechanical function in mouse and man.

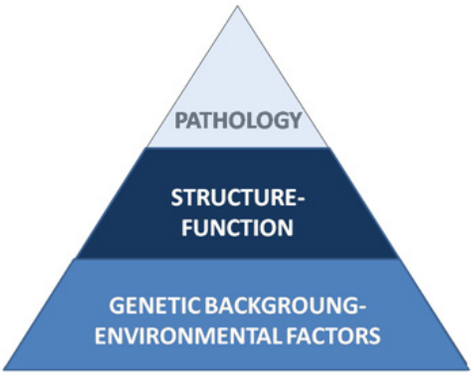

Figure 1. Hierarchical structure for studying human-animal pathology. Fundamental to the elucidation of pathological mechanisms is the detailed understanding of the structure and physiological function of tissues-organs as determined by their genetic background, or as influenced by the local environment.

2. MRI of the mouse: Challenges for cardiac image-based mouse phenotyping

2.1. The mouse as a research model

The mouse emerged as an attractive animal research model following the rapid advances in experimental molecular biology techniques that allowed targeted mutagenesis in single genes [Capecchi 1989], in addition to the tremendous success for extraction, manipulation, and use of embryonic stem cells [Koller 1989]. Practical and ethical advantages were also associated with mice, such as their stable genetic lines, immune system, short gestation periods, low cost, and ease of use. Initial research strides were supported by US National initiatives including the Human and Mouse Genome projects administered through the National Institutes of Health (NIH) for cloning and mapping the entire human and mouse genomes [Collins 2003, Gregory 2002], efforts that were successfully completed in 2003.

Todate, multiple thousands of different knockout mice have been constructed (by individual Institutions, Laboratories, or National or International Consortia), most of which affect cardiovascular function. As attempts to match genotype to phenotype continue, an increasing number of knockout or loss-of-function mice is expected to be generated.

However, despite the usefulness, practicality, and low costs associated with the study of the mouse, important genetic, developmental, morphological, and physiological differences exist between mouse and man [Doevendans 1998, Schaper 1998]. The section that follows addresses succinctly common and distinctly differing features and functional differences in mouse and man and discusses the mechanisms of anesthesia effects on the mouse physiology and cardiac contractile machinery.

2.1.1. Genetic background and gene homology

Through various structural genomics attempts to map and compare human and mouse genomes [Schaper 1998, Gregory 2002], an overall homology of more than 85% and an identity of more than 80% were recorded [Schaper 1998], suggestive of the increased conservation during differentiation of the two species. Based on such findings, it is shown that the homeobox (hox) genes (transcription factors responsible for development), other transcription factors that bind to promoters encoding acute phase genes, and heat shock proteins, exhibit increased identity with humans. Based on Schaper et al. [Schaper 1998], however, structural genomics shows that (except primates) all other species (including mouse, rat, horse, bovine, etc) are equidistant from man, and evidence is thus inconclusive for the choice of the best species (based only on genetic homology and protein identity) for assessment of cardiovascular function and dysfunction.

2.1.2. Developmental and morphological differences between mouse and human

Cardiac dimensions

Indicatively, the human heart weighs around 250-300 g (left and right ventricular [RV, LV] and atrial chambers), and has an intrinsic rhythm of around 60-70 beats per minute (bpm), while the murine heart has a weight of 0.2-0.3 g and beats at a rate of 600-700 bpm. Additionally, the most evident external morphological difference between the adult mouse heart and the human heart is its shape and size (Figure 2). Developmental differences also exist; human development starts during the 3rd week of gestation and lasts approximately 7 months to complete, while mouse cardiac development spans a little more than 2 weeks. At human birth, most of the cardiac organ development has been completed while in the infant mouse cardiac development may still be in progress.

Cardiac anatomy

No major differences exist in the outer morphology, ventricular structure, or valves. Noted differences exist, however, in atrial and venous parts. Specifically, the left superior caval vein drains directly into the right atrium in the mouse, whereas the pulmonary vein has an opening in the left atrium [Doevendans 1998], and a secondary atrial septum is lacking

[Webb 1996]. While availability of data on the cardiomyofiber structure is scarce, a prior publication [McLean 1992] indicates some fiber orientation differences, primarily on the middle layer of the myocardium.

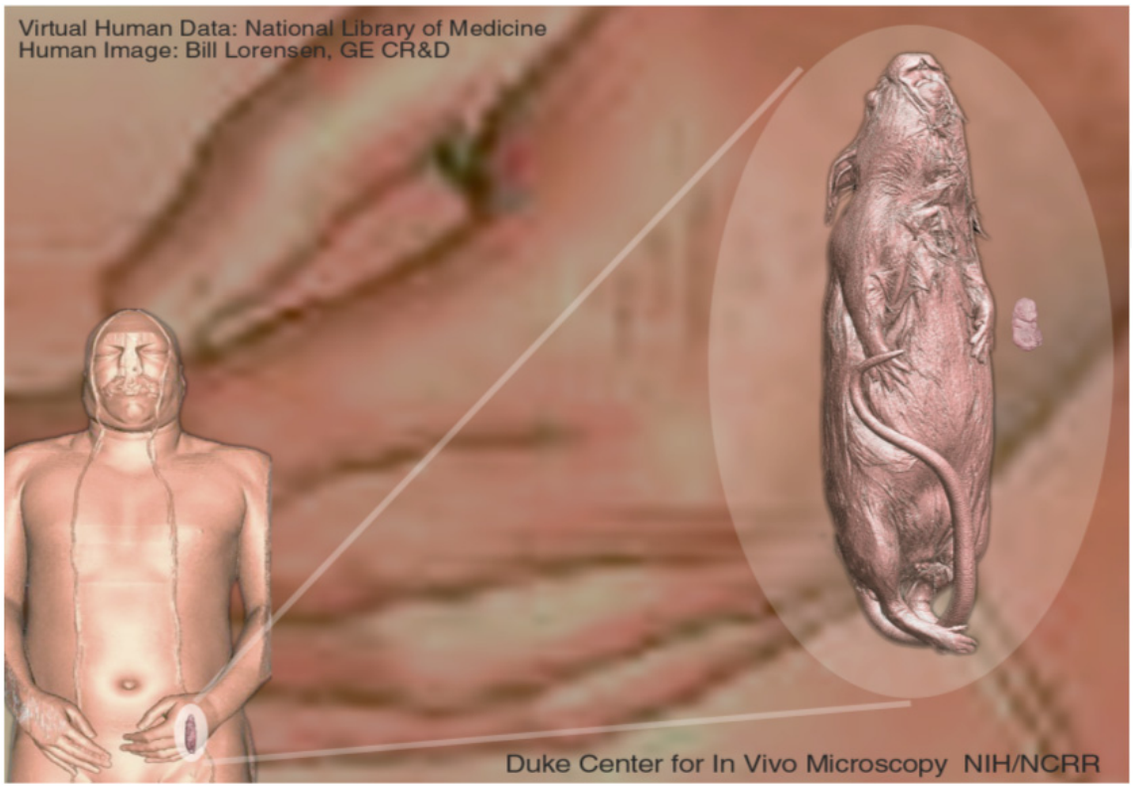

Figure 2. Relative size scales of the human, adult, and mouse embryo [Courtesy of the Duke Center for In Vivo Microscopy, an NIH/NIBIB National Biomedical Technology Resource Center (P41 EB015897)].

Prominent differences also exist for the conduction system and coronary anatomy. In contrast to the human where the sino-atrial (SA) node is distinctly located on the right atrium, in the mouse it lies on the superior vena cava (SVC), at the juncture of the SVC with the right atrium. Coronary anatomy exhibits branching of a septal coronary artery from the left coronary system supplying the left anterior ventricular wall, while the right coronary artery branches into a right coronary and a circumflex vessel supplying the posterior ventricular wall [Doevendans 1998].

Cellular size and content

Cardiomyocytes are reported to have lengths of approximately 80-100 μm along their major axis, and lengths of 10-20 μm along their minor axis [Doevendans 1998, Smaill 1991). Eighty-five percent (85%) of the total number of cardiac cells (amounting to 7-10 million approximately) are interstitial while the remaining 15% that represent cardiomyocytes occupy 90% of the available total ventricular tissue volume [Doevendans 1998]. Also important is an increased capillary to fiber ratio (of the order of 1.4) in the mouse, a direct necessity for the higher energetic and metabolic demands compared to rats, canine, or humans, (with a fiber ratio of the order of 1-1.1) [Sabbah 1995, Przylenk 1983, Olivetti 1989,

Doevendans 1998]. The duration of the cell cycle (once G1 is entered) is reported to be almost the same in mouse and man [Schaper 1998].

2.1.3. Functional physiological differences

Cardiovascular metabolism

Energetic requirements in biological organisms are often assessed by their oxidative capacity, myosin ATPase and SERCA activities [Blank 1989] with a commensurate increased demand in small animals, such as rodents. In compensation of such increased energetic demand, an increased volume density of mitochondria is reported by Doevendans et al. [Doevendans 1998] in mice (37.9%) compared to humans (25.3%), with similar myofibril density (approximately 50%). However, recent findings by Phillips et al. [Phillips 2012] argue in favor of a constant density of mitochondria across species (approximately 21%), yet an increased enzymatic activity of mitochondrial enzymes in mice and a smaller dynamic range of metabolism is reported. Also of interest are the relative patterns of cardiac myosin chain isoforms ($\alpha\alpha$, $\beta\beta$, $\alpha\beta$), a mouse $\alpha\alpha$-isoform compared to a human-$\beta\beta$ isoform dominance [Sheuer 1979], and a developmental switch in mice compared to humans, resulting in higher myosin ATPase activity. Noteworthy and more important is the increased basal activity of metabolic enzymes (Complex V) [Phillips 2012] and the smaller energetic reserve in mice compared to humans [Blank 1989, Phillips 2012], raising concerns for the appropriateness of the mouse as a proper model for comparative pharmacologic (doputamine, dipyridamole) stress studies in ischemia-infarction-reperfusion models, compared to human disease [van Rugge 1992, Wiesmann_Circ_Res 2001, Williams 2001].

Perfusion, angiogenesis-collateral flow, coronary reserve

Based on the extensive number of literature publications that focused on the elucidation of the basic principles of cardiovascular physiology (during the early and latter half of the 20th century), including the autoregulation of blood flow in rats and canine [Feng 2001, Sandgaard 2002], important differences exist in mouse and man with regard to perfusion, capillary density [Stoker 1982, Rakusan 1994], total blood volume (2.5 ml in the mouse compared to 400-500 ml in humans), relative distribution of blood flow in the capillary bed and redistribution capability subject to stimuli (temperature, anesthesia) [Barbee 1992, Rosenblum 1997, Sarin 1990, Constantinides 2011], angiogenetic capacity and formation of collateral vessels, as well as the resting coronary reserve, as factors that primarily project to ischemia-reperfusion studies (or other cardiovascular pathology models) and comparative analyses between pigs, canine, and man.

In vivo cardiac function

While direct comparative studies between mouse and man are still few, nevertheless published results favor similar hemodynamic and global cardiac functional indices, including blood pressure [Janssen 2002, Constantinides, 2011], inotropic (ejection fraction [EF], maximum developed ventricular pressure rates - dP/dt_{max}, stroke work (SW), preload adjusted maximum power (PAMP), Preload recruitable stroke work (PRSW), end-systolic

elastance (ES), and the end-systolic pressure volume relationship) and lusitropic (minimum developed ventricular pressure rates - dP/dt_{min}, Weiss and Glantz relaxation constants, and the end-diastolic pressure-volume relationship), left ventricular contractile indices [Constantinides_ABME 2011, Doevendans 1998]. Recent MRI findings also support similar torsional patterns, as reported by normalized (to left ventricular lengths) twist and torsional angles [Henson 2000, Zhou 2003, Liu 2006, Zhong 2010], however, limited and less steep responses in the force-frequency relationship-response of the mouse compared to humans [Stull 2002] refers to altered calcium kinetics [Stuyvers 1997] and handling under stress.

Integrative physiological control

In consideration of the various morphological and anatomical comparisons listed, the murine cardiovascular system (under normal physiological conditions) resembles relatively closely evoked responses in larger mammals. As mentioned, numerous cardiovascular indices in mice match corresponding values in rats and humans, predicted by allometric scaling laws.

At the integrative physiological level, the major blood pressure regulating systems, namely the baroreceptor reflex [Ma 2002] and the renin-angiotensin system (regulating electrolyte balance) [Cholewa 2001] seem to resemble closely those in larger mammals.

However differences do exist, including the increased sensitivity of blood pressure to anesthesia and temperature, especially under conditions of stress [Barbee 1992, Rosenblum 1997, Sarin 1990, Janssen 2004, Constantinides_ILAR 2011], higher resting cardiac sympathetic tone [Janssen 2000, Janssen 2002], neurotransmitter release [Ehmke 2003], and others.

Allometric scaling of function, energetics, and metabolism

Overall, under physiological conditions, evidence supports that bioenergetically and hemodynamically the mouse scales linearly with larger mammals and humans [Dobson 1995, Nielsen 1958, Phillips 2012], exhibiting a similar maximal aerobic capacity across species [Phillips 2012]. Preliminary evidence for allometric scaling to heart size in mechanical kinematic performance has also been presented [Popovic 2005, Zhong 2010] supported by preliminary comparative mouse-human results in this present work.

Given all considerations, extrapolations of inferences from mice to man is appropriate under physiological conditions, however, similar attempts in pathological models or states may be indeed risky.

2.2. The impact of anesthesia for mouse studies

Even if advances in telemetric techniques have allowed the pursuit of mouse studies under conscious conditions to a large extent, most of the research (terminal, invasive, or non-invasive imaging) studies utilize anesthetics. Anesthetics, however, are known to cause severe cardio-depression [Hart 2001] with adverse physiological effects on hormonal release, centrally to the heart and peripherally to the vasculature [Price 1980, Ohnishi 1974] at the cellular level, affecting calcium entry through L-type Ca^{2+} channels, the calcium

binding sensitivity of the contractile proteins to calcium, on conduction and excitability, and possibly on other sarcoplasmic reticular sites [Price 1980]. Also prominent are effects on the central and peripheral nervous system, but most notable are effects on the metabolism (through mitochondrial vasomotor changes in coronary circulation and perfusion, vasodilation, and blood flow changes in the microvasculature [Kober 2005], possibly synergistic to Nitric Oxide), and the decoupling of oxidative phosphorylation manifested through myocardial oxygen consumption changes.

2.2.1. Mechanisms of anesthesia action

Linus Pauling [Pauling 1952] was one of the first scientists to attempt to explain the molecular and cellular mechanisms of action of anesthetics. Nevertheless, his proposed theory on clathrate formation post-anesthesia administration, proved inaccurate. With recent advances in molecular biology, new published evidence justifies the prominent role of the cellular chlorine channel as a mediator for anesthesia induction and maintenance [Brunson 2008, Maze 2008]. Specifically, hyperpolarizing chlorine channel currents lead to inhibition of cellular excitability and hypnotic action. It appears that one of the major hypnotic action centers is the locus coeruleus in the central nervous system, with mediatory action referred to the α_2-adrenergic receptors via cyclic-AMP-mediated transduction pathways.

At the integrative physiological level, the effects of anesthesia target multiple cellular sites (Figure 3) and thereby often lead to cardio-depression. Major effects include their potency in inducing vasodilation of both the cerebral and coronary vasculature [Toyama 2004] leading to increased perfusion. A rapid hyperglycemic effect is often expressed (primarily via the sympathetic nervous system innervating the liver) causing immediate hormonal (catecholamine) release from the adrenal medulla [Durand 2009]. Glucose metabolic rates are also down-regulated (via inhibition of ATP synthesis in mitochondria), eventually leading to impairment of glucose tolerance (mediated via enzymatic protein activity in the liver). Also observed is an eventual oxidative phosphorylation decoupling.

2.2.2. Types of anesthesia

Widely used anesthetics for animal research are categorized into injectable (such as Ketamine/Xylazine, propofol, lidocaine, nembutal) and inhalational (such as isoflurane, halothane, and sevoflurane). Hedlund et al. [Hedlund 2008] and Brunson et al. [Brunson 2008] have published excellent summaries of the different types of anesthetics used for rodents to which the reader is referred.

2.2.3. Basal physiology and maintenance

While anesthesia usage causes physiological changes [Hildebrandt 2008], proper protocols and administration methodologies (type, dose) can achieve optimal conditions of animal study, maintain animal stability and homeostasis, and minimize time-induced accumulated

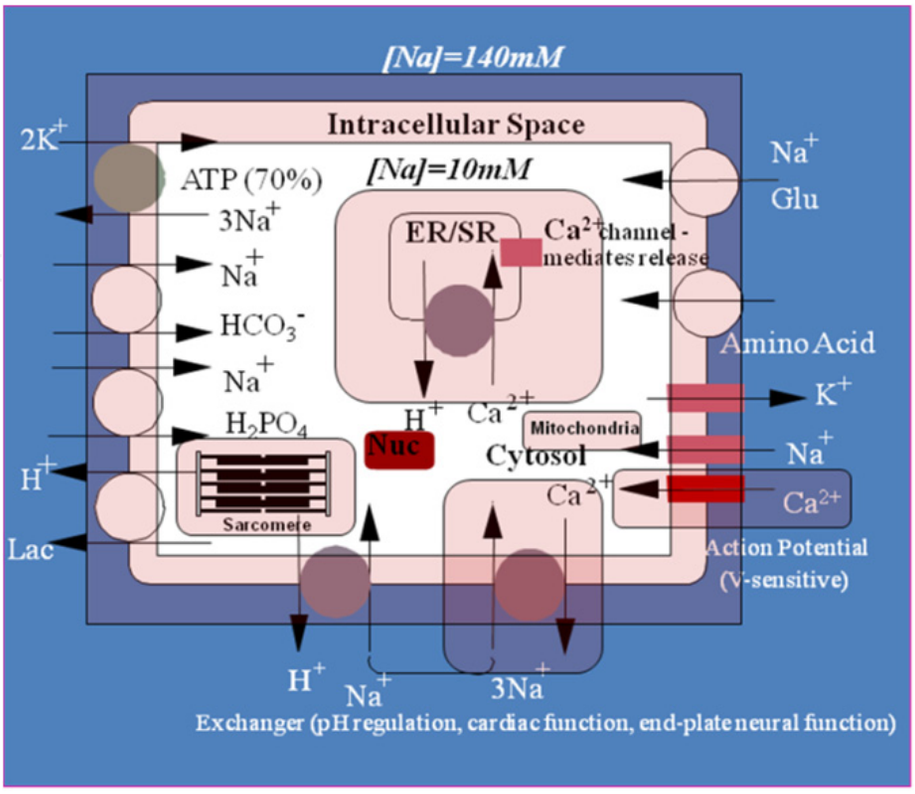

Figure 3. Schematic representation of a typical myocyte with indicative (highlighted) target sites of inhalational anesthesia.

effects, especially for prolonged imaging studies often exceeding 45 minutes in duration. Apart from physiological indices of hormonal release, respiration and metabolism, carefully controlled cardiac indices (such as heart rate, ejection fraction, arterial pressure, and heart variability) ensure proper conditions of study of the cardiovascular system avoiding detrimental hypotension-induced blood volume changes, metabolic and contractile down-regulation, and arrhythmogenicity. Heart variability (HRV) analyses have also been applied for phenotypic screening of transgenic mice, study of heart rhythm mediators through signaling pathways as well as the effects of pharmacologic intervention on intrinsic heart rhythm and arrythmogenesis [Thireau 1997, Bernston 1997, Gehrmann 2000]. Standardization of HRV analyses tools for mice have, however, been limited due to the numerous data acquisition types and analysis techniques employed. Most importantly, variability of HRV is dependent on the type of anesthesia being used, that may also be further influenced by anesthetic balancing agents such as nitrous oxide (N_2O), medical air, and oxygen. Interpretation of HRV results has also been difficult [Hoit 2004], due to their dependence on a number of factors including aging, posture, circadian variability, and the duration of the sampling periods used, with recent evidence supporting the fact that the primary contribution of autonomic activity in the mouse is due to the sympathetic tone, in contrast to the parasympathetic vagus contribution [Janssen 2002, Janssen 2000, Constantinides_IEEE 2010].

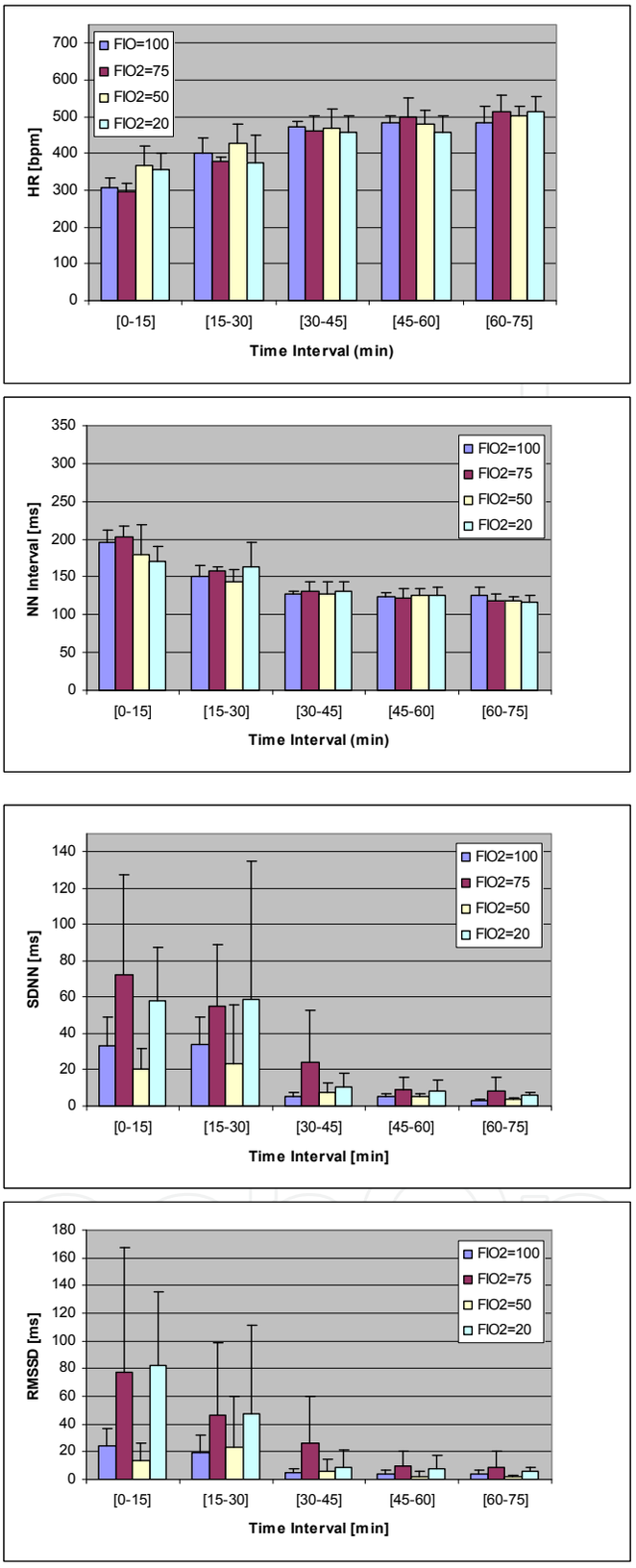

Figure 4. Heart rate variability indices at varying FiO_2 values. (Top) HR, R-R intervals (NN), (bottom) SDNN, and RMSSD variation. [Reproduced from Constantinides C et al. [Constantinides_IEEE 2010] with IEEE permission].

Despite such previous work, the extent of the contribution of sympathetic and parasympathetic tone to heart rate (HR) and HRV in the mouse is still a matter of debate. Recent, carefully controlled studies based on the level of anesthesia and additional factors that relate to animal preparation indicate that overall, HRV is expected to be generally lower during anesthesia in comparison to the conscious state. Indicative in HRV is an SDNN reduction under FiO_2 conditions at 50% but also a noted increase in the standard deviation of averages of all normal R-R intervals (SDNN) and the square root of mean squared differences between adjacent normal R-R intervals (RMSSD) as a result of N_2O administration. Variation of FiO_2 seems to result in prominent effects only at specific levels (50, 100%). Since HRV indices are determined by an inter-play between both mechanical and neural factors, the exact mechanisms responsible for this effect are still unknown.

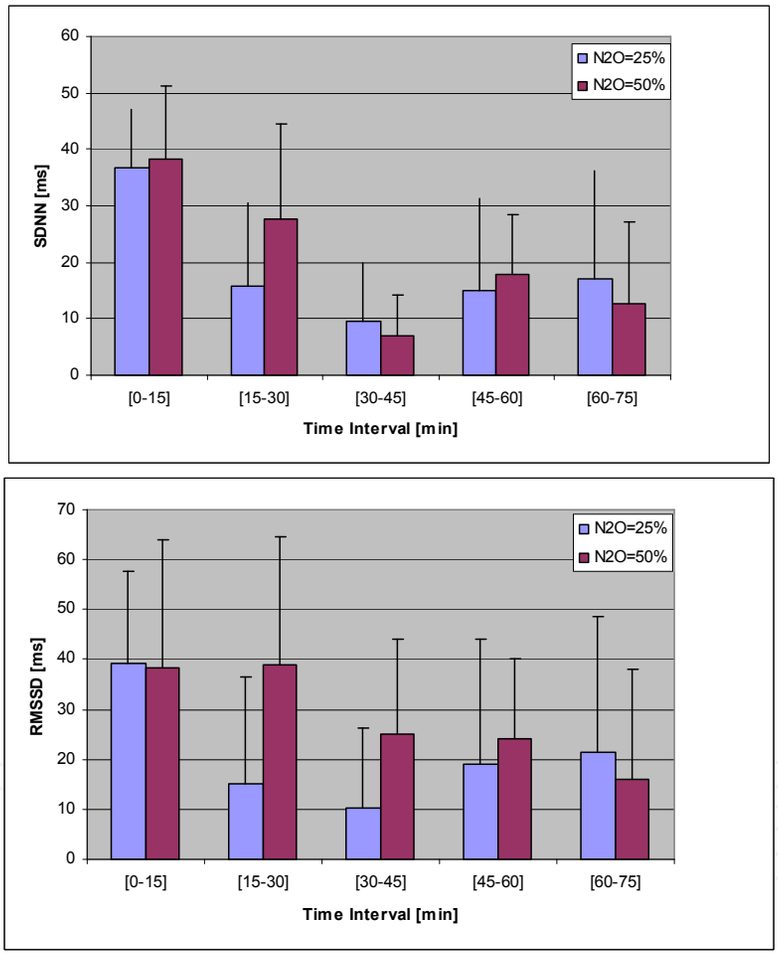

Figure 5. Heart rate variability indices with varying N_2O/O_2 values (25-75% and 50-50%) at different time intervals post-anesthesia induction. (Top) SDNN and (bottom) RMSSD variation (n=3-6 per group). [Reproduced from Constantinides et al. [Constantinides_IEEE 2010] with IEEE permission].

Overall, the major practical benefit is that the protocol described for physiological studies of mice under anesthesia has the potential for high reproducibility in diagnostic modalities including MRI, microCT, ultrasound, and microPET. Elicited results show that the optimal ISO anesthetic regimen for mice is a dose of approximately 1.5% v/v mixed with 25–50% O_2

and 75–50% N_2O. However, despite the optimization of murine physiological conditions under anesthesia, it is yet not possible from this study to determine whether the mechanism of action involves transient sympathetic activation, steroid release, a direct effect of ISO, or a combination of such effects. The overall effects of ISO may be the result of opposing vasodilatory and vasoconstrictive effects either directly (vasodilation) or secondary to an anesthesia-induced decrease of the heart's metabolic demand. Surely, the major limitation of all studies under anesthesia is that a noted cardio-depressive effect on basic cardiovascular function exists, compared to the conscious state.

3. MRI cardiac imaging: The current status and future perspectives

Mouse cardiac MRI emerged as a logical consequence to the human and mouse genome mapping initiatives and parallel developments and advances in human cardiac MRI in the late 1980's and early 1990's, focusing on establishing MRI as the 'one-stop-shop' in clinical practice. Correspondingly, technological advances and developments of novel hardware and pulse sequences were fairly limited, merely revolving on the scalability of existing technology to match smaller field-of-view acquisitions for mouse and rat imaging. Manning et al. [Manning 1990] and Shapiro [Shapiro 1994] first reported cardiac MRI-based LV mass estimations, and Siri et al. [Siri 1997] the first mouse cardiac imaging results from a 9.4 T system. Subsequent to such early studies were the first quantitative studies of function [Ruff 1998] and myocardial mass in diseased mice post-hypertrophy induction using the β-adrenergic agonist isoproterenol (ISO) [Slawson 1998]. Despite attempts early on to utilize conventional 1.5T clinical systems to conduct mouse cardiac MRI [Franco 1998], it was soon realized that dedicated, high field, high resolution mouse systems were necessary for imaging, a realization that drove technological evolution and migration to field strengths of 4.7-11.7 T systems [Wiesmann 1998].

Collectively, efforts over the last 14 years targeted the study of global [Ruff 1998, Wiesmann 1998, Wiesmann 2002, Schneider 2003, Zhou 2003] and regional cardiac function [Epstein 2002, Zhou 2003, Heijman 2004, Zhong 2010] in transgenic and wildtype-littermate control mice as a basis for image-based phenotyping [Wiesmann 2000, Wiesmann_Card_Magn_Reson 2001, Chuang 2010]. They also addressed models of disease (ischemia-infarction-reperfusion [Nahrendorf 2000, Ross 2002] and heart failure [Wiesmann 2002, Schneider 2003, Schneider 2004]). During the evolution of such prior attempts, noted advances in the mouse physiological status and its maintenance in high-field horizontal or vertical systems [Schneider 2003, Schneider 2004, Frydrychowicz 2007], and electrocardiographic (ECG) and respiratory gating strategies have been reported [Cassidy 2004, Bishop 2006, Hiba 2007, Heijman 2008, Bovens 2011] over the years. Other prominent work on mouse MRI also includes cardiac studies in imaging-based embryogenesis and development [Johnson 2002, Wiesmann 2000], perfusion [Kober 2005, Streif 2005], metabolism [Chacko 2000, Weiss 2002], coronary artery imaging [Ruff 2000], and stress testing [Williams 2001].

Only recently have efforts been completed to quantify the murine motional patterns and regional cardiac mechanical function [Zhou 2003, Streif 2005, Zhong 2010] towards the study

of function and dysfunction using advanced techniques, including black-blood CINE [Berr 2005], spin-tagging [Epstein 2002, Liu 2006], DENSE [Zhong 2010], and HARP [Osman 1999, Kuijer 2001]. This section discusses some of the fundamental aspects of mouse preparation, positioning, physiology and its maintenance during MRI, advances in hardware and pulse sequence acquisitions, image processing techniques, and global and regional cardiac phenotyping, as these are complemented with recent findings from our group.

3.1. Mouse physiology - Maintenance and stability during MRI

Even if physiological protocols are easier to optimize on the bench, murine cardiac MRI imposes additional stringent challenges that relate to the animal's heart rate, pressure monitoring, and thermoregulation [Schneider 2004, Hedlund 2008, Constantinides_ILAR 2011]. While most research sites are equipped with commercial mouse imaging systems, a number of adjustments often need to be implemented to ensure proper physiological maintenance (including, but not limited to, computer controlled ECG, breathing, temperature monitoring systems and MR-compatible [fiber-optic and other] devices) [Figure 6]. Often specially designed negative-feedback air-flow systems are interfaced with closed-bore scanner systems to facilitate fast and efficient bore air-heating, compensating for the lower bore temperatures due to the cryogenic environment of the magnet and gradient coils.

Proper mouse positioning almost always requires specially designed cradles to fit imaging probes (often constructed on specially designed casings that fit in fast-switching, high-slew rate gradient inserts) and scanner high-performance RF coil and gradient inserts.

Mouse cradle designs have evolved in complexity over the past 14 years and include those custom-made and commercially available types. Most of them are customized to allow mouse placement in prone and supine positions, placement of non-magnetic metallic or carbon-fiber ECG electrodes on the front paws and limbs, a rectal probe and an inflated air-bellow, for temperature and respiration monitoring [Figure 6]. Also of importance is the administration of anesthesia gases, often accomplished via a nose cone (with mice being obligatory nostril breathers), with tubing that connects to a vaporized-flowmeter device system (freely breathing [Schwartz 2000]), or directly to a ventilator device (achieving time-synchronous ventilation) as reported previously [Gilson 2005, Constantinides_ILAR 2011]. Special arterial or venous lines (tail vein, carotid vein or artery) are often adapted to allow pharmacologic infusions or arterial/ventricular blood pressure monitoring [Constantinides_ABME 2011]. Intraperitoneal injections are also preferred for anesthesia or contrast agent infusions.

Maintaining the mouse under optimal physiological conditions for a 60-90 minute MR imaging study, is a formidable and challenging task. Often, the HR value may be misleading as an indicative biomarker of proper physiological status (masking an underlying hypotension or cardiac contractile down-regulation [Constantinides_ILAR 2011]), especially after prolonged anesthesia exposure, excessive infusion of electrolytes (for blood volume maintenance), or following pharmacologic challenges. Therefore, care must be exercised in the initial induction, proper inhalational anesthesia administration, proper acclimatization of the animal to its imaging environment, and careful control and monitoring of its temperature and

other critical physiological parameters (including, but not limited to HR, coefficient of variation [CV], mean arterial pressure [MAP], blood pH, glucose, and insulin) maintaining homeostasis throughout the study as shown in Table 1 [Constantinides_ILAR 2011].

Figure 6. Physiological monitoring of mice during MRI using a dedicated recording system and the Labview software; (b) specially designed mouse positioning cradle, and (c) RF coil-mouse cradle assembly for a small-bore, high field animal scanner.[Photographs acquired from the Center for In Vivo Microscopy at Duke University Medical Center, an NIH/NIBIB National Biomedical Technology Resource Center].

3.2. Advances in specialized hardware for high field animal MRI

3.2.1. High field magnets

While gradient and RF coil technology spans numerous decades of history (as early as Paul Lauterbur's ground-breaking inception of zeugmatography [Lauterbur 1973]), the stringent technical requirements imposed by the mouse physiology for cardiac imaging have led to optimization of prior technology or to recent introductions of new technologies, as reviewed and discussed briefly in this section. Interestingly, large-bore high-field systems emerged during the past decade at field strengths spanning 4.7, 7.1, 9.4, and 11.7T maintaining, however, the same design technology as originally developed for human superconducting systems in the late 1980's and 1990's.

Anesthesia/Inhalation Mixture		HR [bpm]	CV_{HR}	MAP [mmHg]	CV_{MAP}	t_{RR} [ms]	pH	Glucose [mg/ml]	Insulin [ng/ml]
ISO=1.0 %	O_2=100 %		14±2 (N=7, M)		13±3 (N=7,M)		7.3±0.1-7.4±0.1 (N=9/5, M)	176.3±26.1 - 188.8±11.1 (N=4/5, M)	3.4±0.5-4.2±0.9 (N=4/5, M)
ISO=1.5 %	O_2=100 %	478±11.4 (N=7,M)	11±1 (N=7, M)	92±2 (N=7, M)	8±2 (N=7,M)	114-134ms (N=4, M)			
ISO=2.0 %	O_2=100 %		14±3 (N=7, M)		33±2 (N=7,M)		7.3±0.1-7.3±0.2 (N=9/6, M)	139.4±30.1 -192±11.9 (N=4, M)	3.54±0.3-4.24±0.6 (N=4, M)
ISO=1.5 %	O_2=75%		10±2 (N=7, M)		25±6 (N=7,M)				
ISO=1.5 %	O_2=50%	475±21.6 (N=6, M)	9±1 (N=6, M)	90±13 (N=6, M)	6±2 (N=6,M)	108-150ms (N=3-6, M)			
ISO=1.5 %	O_2=20%		8±1 (N=5, M)		10±4 (N=5,M)				
ISO=1.5 %	O_2=50% N_2O=50 %	490±15.0 (N=5, M)	10±2 (N=5, M)	93±3 (N=5, M)	6±3 (N=5,M)	114-124ms (N=3-4, M)			
ISO=1.5 %	O_2=75% N_2O=25 %	516±8.7 (N=5, M)	7±2 (N=5, M)	94±3 (N=5, M)	10±3 (N=5,M)				

Table 1. Summary of various cardiovascular and biochemical physiological indices of anesthetized mice using Isoflurane from bench studies. Stable mouse responses were obtained under both bench and scanner experimental conditions for periods spanning 1-1.5 hrs post-induction. [This table originally appeared in Constantinides C et al., Effects of Isoflurane Anesthesia on the Cardiovascular Function of the C57BL/6 Mouse, published in ILAR e-Journal 52(2), available online at *http://dels-old.nas.edu/ilar_n/ilarjournal/52_2/PDFs/v5202e-Constantinides.pdf*].

3.2.2. Gradient coil technology

The requirements for increased spatial resolution acquisitions (of orders matching cellular size of approximately 100-200 μm^3) led to fast switching, high-amplitude (up to 1000 mT/m), high-slew rate (up to 11250 mT/s) gradients (exhibiting linearity of better than ±3-5%/mm) for ex-vivo constructions of atlases [Johnson 2002] or in-vivo high-resolution isotropic cardiac imaging [Bucholz 2008, Perperidis 2011]. Often associated with extra inserts (of approximately 6-20 cm in inner diameter), such gradients impose further spatial restrictions in animal placement and monitoring during cardiac imaging. However modern, commercially available systems are often equipped with actuator-controlled manual or computerized cradle positioning systems.

3.2.3. RF coils

In a similar fashion to the evolution and migration of magnet and gradient technology from human to mouse applications, advances were noted in RF coils. Of all three hardware components (magnets, gradients, transmit/receive coils), RF coils received most of the attention of the research community for mouse cardiac MRI [Doty 2007]. Despite the use of simple resonant coil loops for cardiac studies early on, image-based phenotyping attempts [Wiesmann 2000, Wiesmann_Card_Magn_Reson 2001] redirected attention to high-throughput imaging and to the deployment and construction of multiple-mouse phased arrays [Bock 2003, Ramirez 2010]. Availability of multiple receivers, in combination with parallel imaging techniques (SENSE, GRAPPA), have reinforced attempts for high-throughput mouse acquisitions at high fields [Sosnovick 2007, Schneider 2010]. More recent developments of scaled-down birdcage coils have provided optimal imaging solutions for single mouse MRI as exemplified by direct comparative studies with simple surface [Markiewicz 2006], planar, and cylindrical spiral multi-turn coils (Figure 7) [Constantinides_Concepts 2011].

Traditionally, RF surface coils reduce the spatial coverage (and hence the field-of-view) compared to volume coils, while maintaining higher local signal-to-ratio (SNR). The limitation for expansion of the spatial region of surface coil coverage (while maintaining or improving SNR), yielded to phased array designs, often in combination with circularly-polarized volume transmit coils. Introduction of alternative coils to phased array designs, such as the one shown presents one of the first attempts to ameliorate such a surface coil limitation, in consideration of the small spatial scales, and the complexity and cost of phased arrays. Additionally, the use of such a surface coil is not prohibitive in terms of its concurrent use with dedicated and specially designed transmit (or receive coil arrays).

Specifically, imaging results showed improved performance of the cylindrical spiral coil in comparison to the flat counterpart. The cylindrical coil has increased field of penetration that allows visualization of the entire lateral and inferior myocardial walls with adequate relative SNR (rSNR). Its performance compares well and outperforms its flat equivalent in septal, inferior, anterior, and lateral myocardial areas (rSNR improvement between 27 and 167%), despite its non-optimal placement and positioning on the mouse (anteriorly and laterally), in this particular case. Its design and response, that clearly exploits the additive effect of the transverse B_1-field component, also compares favorably with a commercially available birdcage coil within the region where the mouse heart resides. However, the birdcage coil exhibits the best performance associated with three to five times higher rSNR values over the entire left ventricular myocardial regions. Promising are anticipated uses and applications of new hyperpolarized cryostat volume (birdcage) coils that have recently become commercially available [Kovacs 2005].

The fact that the constructed coils are transceiver surface resonators, certainly presents a conceptual and practical limitation for their wide-spread use, in the context of inhomogeneous excitation and their ability to allow quantitative cardiac mouse imaging. Direct use of such coils for high field mouse cardiac imaging is likely to result in increased

loading effects between the RF and gradient coil inserts, imposing the need for use of specially constructed isolation shields. The inhomogeneous response of such coils, obviously translates to issues associated with artifacts, imperfect application of magnetization preparation pulses, or biased quantitative measures in cardiac functional and perfusion imaging. Furthermore, flip-angle sensitive techniques, such as fat saturation in cardiac MRI cannot be applied, due to the inherent variations in the flip angle spatial distribution, thereby limiting their potential applications.

3.3. Conventional and new imaging methodologies for mouse cardiac imaging

Similar to hardware developments numerous pulse acquisition schemes migrated from human cardiac applications to the mouse. Nevertheless, a number of new techniques emerged over the years that include cartesian (rectilinear) and radial (spiral, twisted projection, other) data acquisition schemes for fast mouse cardiac imaging. A brief review and analysis of the most-successful imaging and reconstruction practices (fast Fourier and non-uniform data regridding-Fourier transformations) is attempted below.

3.3.1. Cartesian k-space pulse sequence acquisitions

Two were the major types of Cartesian imaging acquisition techniques that migrated from prior human MRI efforts, extensively used for mouse cardiac imaging. They are both gradient echo sequences and adhere to lexicographic k-space or rectilinear sampling and are based on spin-warp imaging. The first, a steady state incoherent pulse sequence, was developed by Haase [Haase 1986] and became known as Fast Low Angle Shot and was dubbed with the acronym FLASH (equivalent to Spoiled Gradient Recalled Imaging, later developed by General Electric). The second type, a steady state coherent sequence known as Steady State Free Precession (SSFP) was developed early on by Carr [Carr 1958], employing ultra-short repetition times (TR) for imaging later adopted in an equivalent sequence with gradients by Hinshaw [Hinshaw 1976] and Frahm et al. [Frahm 1987], a sequence known as Fast Imaging with Steady Precession (FISP) [with the equivalent acronyms of Gradient Refocussed Acquisition at Steady State (GRASS) and balanced Fast Field Echo (B-FFE), as the GE's and Phillip's equivalent versions]. While SSFP was neglected for many years it regained tremendous interest over the last decade following advances in gradient technology in clinical scanners that eventually allowed ultra-short TR imaging.

For mouse cardiac imaging, segmented k-space acquisitions in an interleaved fashion are executed (to allow reconstruction of multi-frame images at spatial resolutions reaching 87 μm isotropic) based on a trigger pulse (prospective [Cassidy 2004, Bovens 2011], retrospective [Bishop 2006, Bovens 2011], or self-gated [Hiba 2007]), or a combination of the ECG and the respiratory [of order of 50-120 breaths/minute approximately] signal (thereby minimizing cardiac motion and respiratory artifacts). Navigator echoes may also be used prior to the gating pulse with a number of preparation pulses (pre-pulses) often executed immediately after the trigger pulse (Figure 8). Such optional pulses may include fat suppression and spectral-spatial pulses for black-blood imaging and/or fat suppression, as well as other prep-pulses including inversion, DENSE, spin-tagging and others.

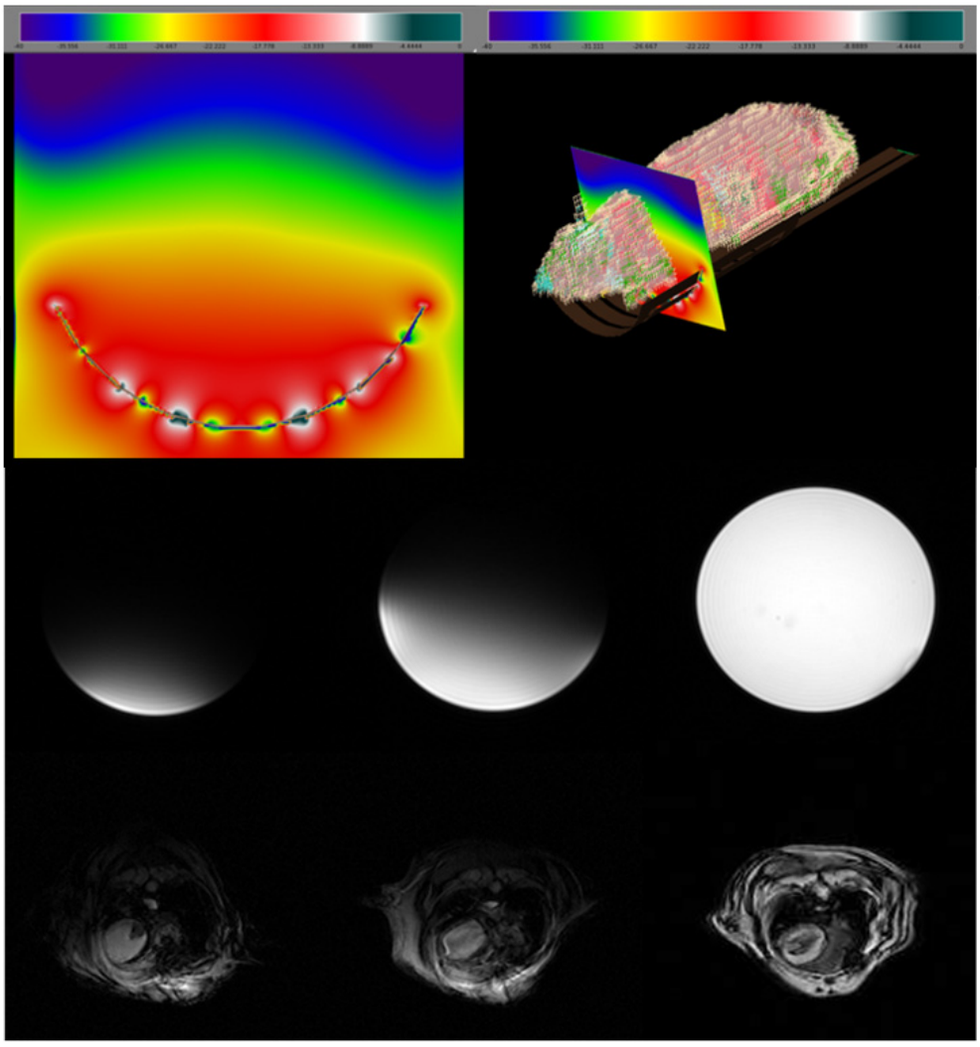

Figure 7. (Top, Left) Mouse XFdtd B_1-field simulation of a four-spiral cylindrical coil under loaded conditions with a mouse computational model (top, right) [color bar varies between 0 – -40 dB];(Bottom) Flat, cylindrical spiral, and birdcage axial phantom response using conventional SPGR pulse sequence acquisitions and corresponding cardiac MRI from each of the three coils in mice post-mortem showing improved performance by the birdcage coil. [This figure originally appeared in Constantinides C et al., Intercomparison of performance of RF Coil Geometries for High Field Mouse Cardiac MRI. Concepts of Magnetic Resonance Part A, 38A(5):236-252, 2011, DOI 10.1002/cmr.a.20225, reproduced with permission from Wiley Publications].

3.3.2. Spiral or non-cartesian k-space pulse sequences

The ultrafast mouse heart rates, even under anesthesia, necessitate fast imaging acquisitions (within t_{RR}=100-120 ms). While Cartesian sampling schemes cover k-space adequately nevertheless, non-rectilinear and spiral k-space acquisitions have gained tremendous interest recently as efficient and fast sampling schemes. Radial acquisition variants by Bucholz et al. [Bucholz 2008], and STEAM-based DENSE encoding followed by interleaved spiral acquisitions proposed by Zhong [Zhong 2010] (Figure 9) are also adopted for mouse cardiac functional imaging.

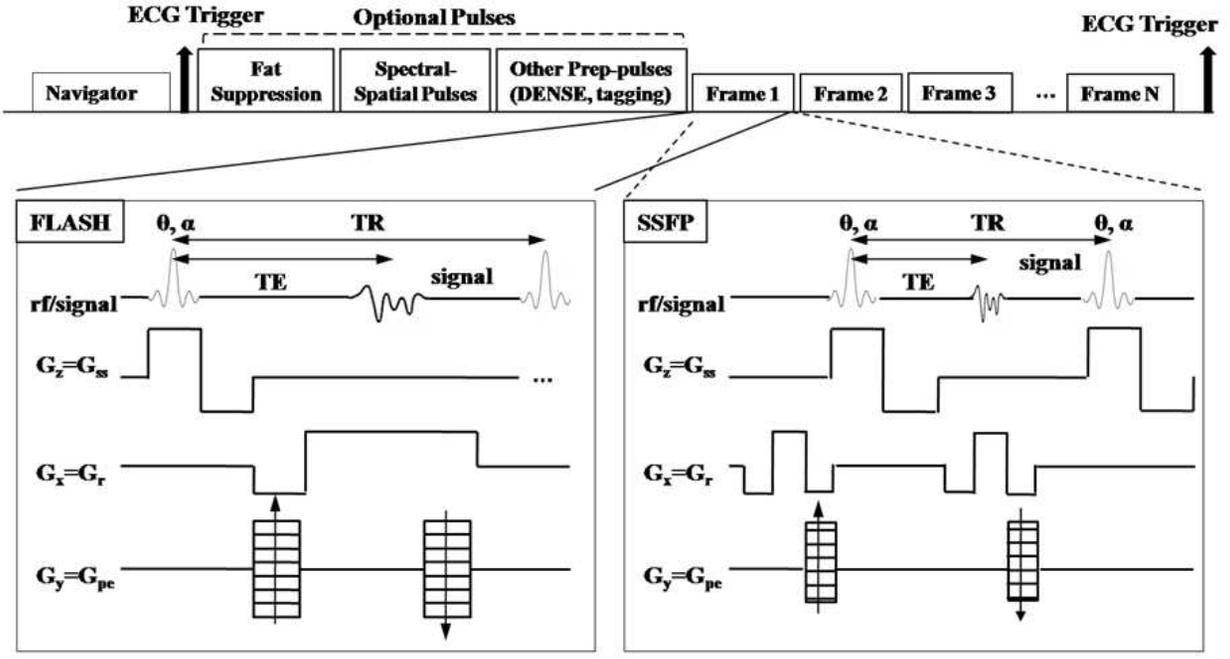

Figure 8. Rectilinear k-space sampling schemes employed for mouse cardiac imaging. (Left) FLASH imaging, and (right) SSFP. Shown on top are optional preparatory pulses and the inherent capability to perform multi-phase CINE acquisition based on the ECG (or a combined cardiac-respiratory) trigger pulse. [G_x, G_r=readout gradient, G_y, G_{pe}=phase encoding gradient, G_z, G_{ss}=slice selection gradient, θ=flip angle, α=RF pulse angle].

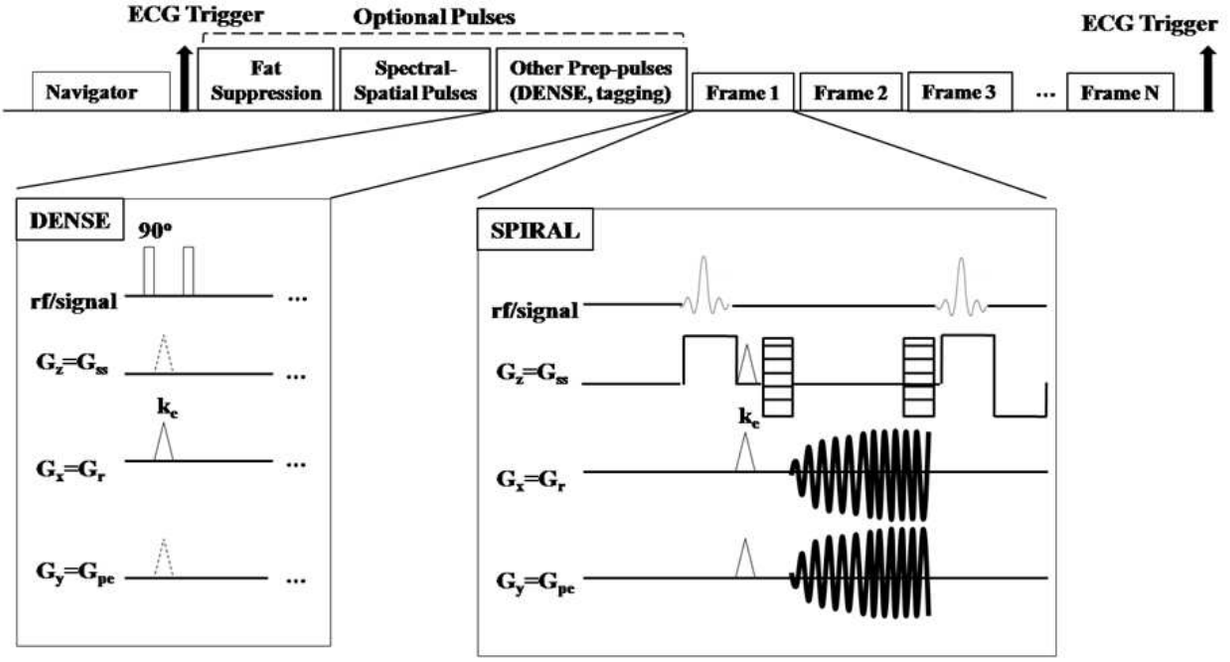

Figure 9. Non-rectilinear k-space sampling for cardiac imaging. Shown is a typical spiral readout scheme used in association with the DENSE (STEAM-based) preparatory pulses. (Left) k_e represents the encoding pulse. The same pulse (un-encoding) is executed during the spiral readout (right). [G_x, G_r=readout gradient, G_y, G_{pe}=phase encoding gradient, G_z, G_{ss}=slice selection gradient, θ=flip angle, α=RF pulse angle].

In summary, numerous practical benefits are associated with mouse cardiac MR imaging, including the non-invasive nature of the technique, the inherent capability to map cardiac morphology and function, for both LV and RV chambers, and their motional patterns. High spatial and temporal resolution imaging can thus be achieved, through execution of high-throughput protocols, yielding direct, accurate estimates of global and regional indices of cardiac function, avoiding any assumptions whatsoever or model-based derivation approaches endorsed by other imaging techniques such as ultrasound.

Despite the extensive use of cartesian imaging with adequate SNR performance and spatial resolution (using FLASH, SSFP, or FISP), 3D acquisition studies maybe more efficiently completed using radial or spiral imaging sequences, especially for dynamic cardiac imaging (with pharmacologic interventions or contrast agent infusions). Nevertheless important and critical drawbacks are associated with such sequences, including the necessity to maintain data density as sampling extends to outer k-space regions, the convoluted and complex reconstructions (often associated with data re-gridding, kernel de-convolution, filtering, and inverse fourier transformation), and inherently lower SNR performance than rectilinear imaging. Thus, the choice between cartesian and radial imaging reduces to a tradeoff between SNR, spatial resolution, and efficiency of data sampling for 3D coverage.

3.4. Image-based phenotyping

Quantitative characterization of ventricular function has become important for the assessment of murine cardiac performance in heart disease [Wiesmann 2000, Wiesmann_Circ_Res 2001, Dawson 2004]. As the manipulation of the mammalian genome becomes routine, it is now possible to generate animal models to study cardiovascular function and dysfunction [Wiesmann_Card_Magn_Reson 2001, Epstein 2002, Epstein 2007, Bucholz 2008, Stuckey 2012]. Critical to successful phenotypic screening of mouse models of the cardiovascular system using MRI are highly efficient four-dimensional (4D) acquisition ex-vivo and [Zamyadi 2010] in-vivo protocols [Bucholz 2010]. Such protocols ought to span the scales of the embryo to the adult, fully-developed mouse, and ought to lead to the reduction of the computational image processing complexity for accurate quantification of motion, global and regional cardiac function, strain, elasticity, and others.

3.4.1. Quantification of global mechanical function and hemodynamic indices

Traditionally, quantification of global hemodynamic indices has been associated with calculation of hemodynamic indices of function. MRI and other diagnostic techniques, (including microCT and ultrasound) are not the only existing techniques to accomplish functional characterization. While ultrasonic techniques are associated with inherent limitations for such quantification [Dawson 2004], microCT has been gaining interest and popularity [Badea 2005]. Miniature catheterization techniques introduced in the late 1990s [Georgakopoulos 1998] have revolutionized cardiac-based phenotypic in transgenic mice. However, their major drawbacks include their invasive nature and other technical limitations [Porterfield 2009, Constantinides_IEEE 2011, Constantinides 2012]. As newly

emerging techniques and applications develop to investigate in-vivo sarcomeric force generation with contrast agents [Constantinides_ABME 2011], the current scientific focus is still on image-based calculations of global indices of function.

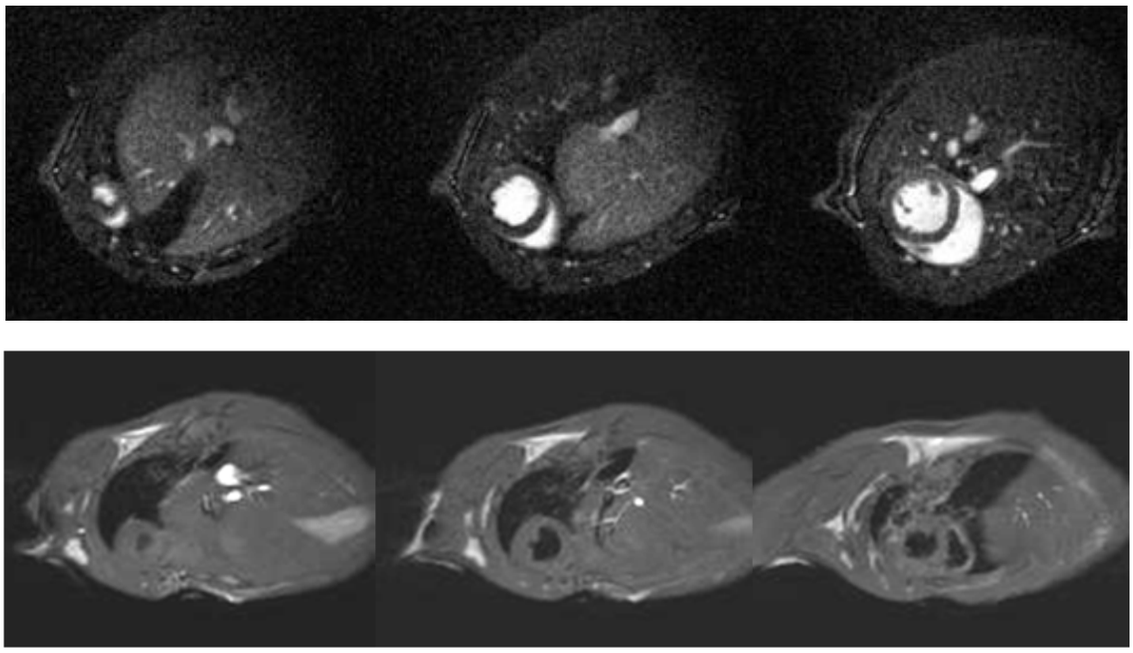

Figure 10. (Top) Typical bright blood true-short axis cardiac imaging at an apical, middle, and basal levels of the C57BL/6 murine heart using a liposomal contrast agent; (Bot) Black-blood spin-echo images of the murine heart at basal, mid, and apical levels.

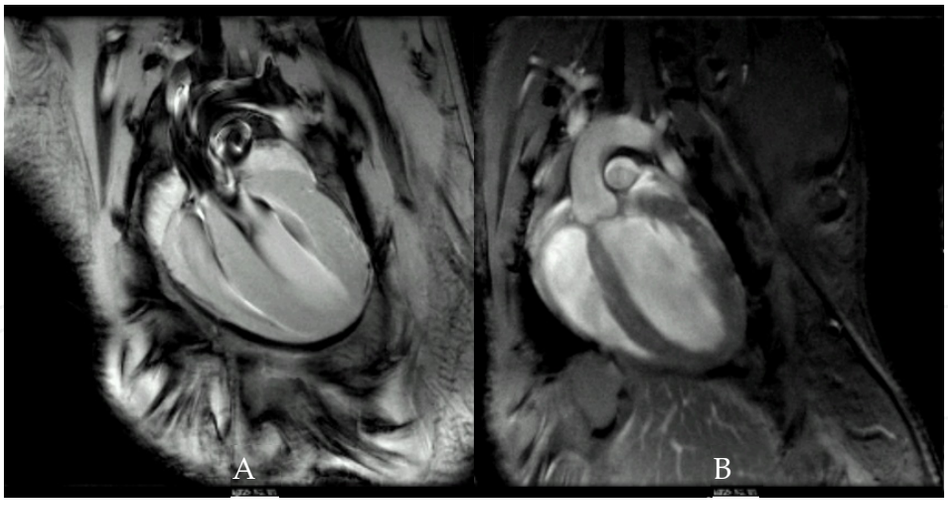

Figure 11. (A) ECG-gated four chamber view of a healthy mouse heart at 78 x 78 μm² in-plane resolution, and (B) corresponding self-gated (retrospective) view of a separate mouse using a navigator echo at the same spatial resolution, at 11.7 T using FLASH-MRI [Images courtesy of Bruker Biospin MRI, Ettlingen, Germany].

Correspondingly, estimated cardiac volumes can easily be computed using standard image processing tools and converted to absolute volume units using the voxel dimension and the myocardial tissue density. Hemodynamic indices such as end-diastolic (EDV) and end-

systolic volumes (ESV), stroke volume (SV), cardiac output (CO), and ejection fractions (EF) can now be routinely calculated according to standard cardiac mechanical functional relations [Constantinides_SBI 2009], based on CINE-MRI (Figure 11). CINE based local contractile function, including estimation of wall thickness, motion and fractional shortening, indicators of systolic function and long-term prognostic biomarkers in dysfunction remain the gold-standard for assessment of motional patterns and cardiac function in small animals due to the excellent soft tissue contrast of MRI and its high spatial and temporal resolution (Figure 12).

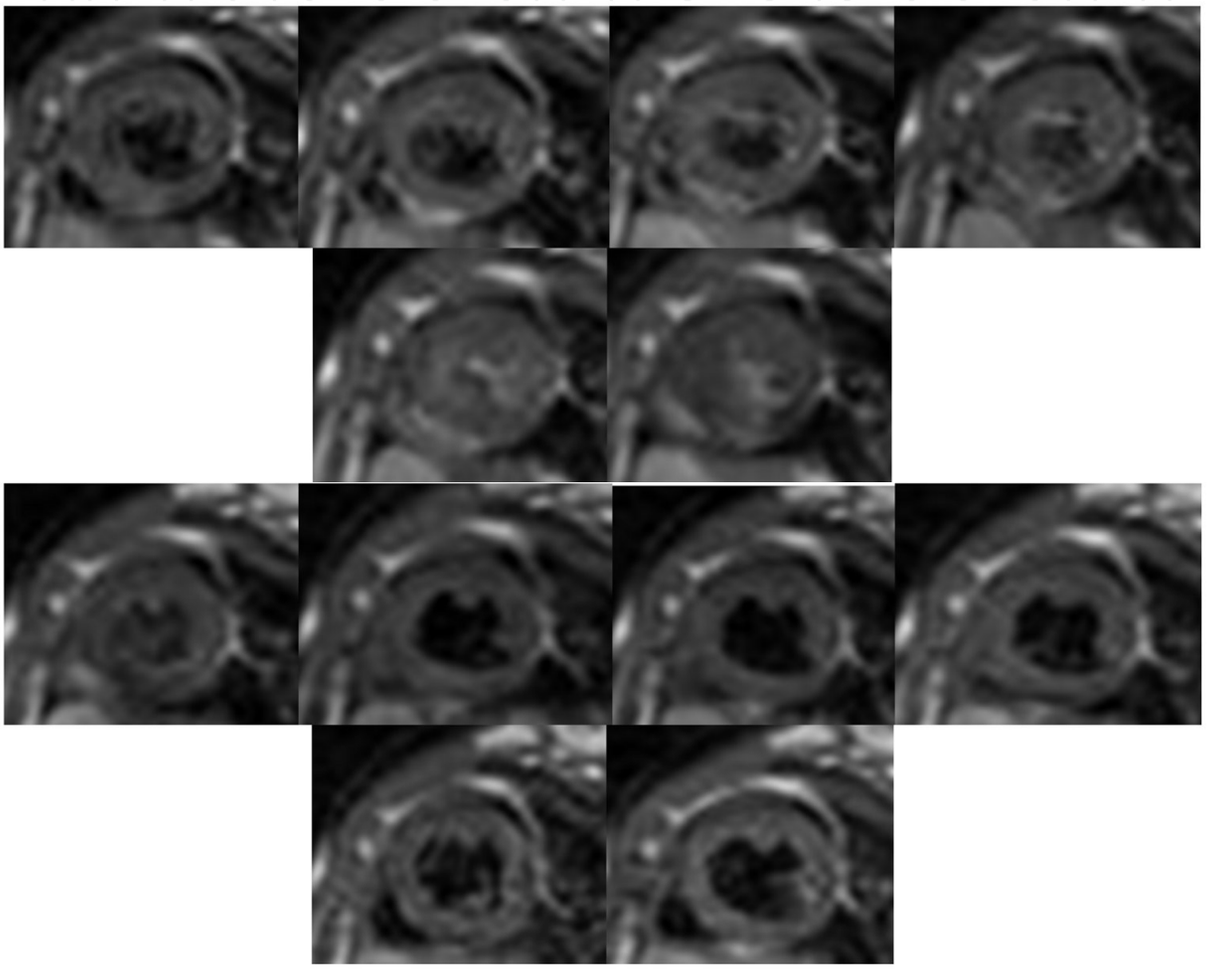

Figure 12. Single-slice, multiphase CINE functional cardiac imaging of the C57BL/6 mouse heart over 12 cardiac phases.

Interstrain morphological and 4D motional variability – Statistical altases

The advances in high-field, high-resolution cardiac imaging techniques, have also allowed the development of atlas-based approaches for the description of anatomical structures and their function [Ali 2005, Sharief 2008] in normal [Ruff 1998, Bucholz 1998, Badea 2005, Zamyadi 2010] and transgenic mice [Chien 2000, Epstein 2007]. Completion of the sequencing of the mouse genome has led to increased requirements for identifying the specific phenotype

elicited post-transgenic modifications and the genetic basis of pathology [Henkelman 2010]. Therefore mouse imaging, combined with probabilistic, statistical atlas constructions and morphometric methods [Zamayadi 2010], is envisaged to play an increasing role in image-based phenotyping and gene expression mapping of genetically altered mice [Ng 2010] in the future. Construction of probabilistic and statistical atlases [Perperidis 2011] can potentially enable the study of murine, global cardiac structure and function with increased quantitative accuracy, identifying modal components of shape variability (from embryogenesis to adulthood), and disseminating components of global mechanical motion. Similar to existing cardiac atlases [Perperidis 1995, Hoogendoorn 2007], these can be population-based instead of single-subject. Prior efforts have focused on modeling cardiac anatomy in humans [Helm 2006] but only limited attempts have been made to construct accurate, high-spatial and high-temporal resolution computerized atlases for mice [Perperidis 2011]. Despite multiple prior efforts with construction of human brain atlases [Young 2009], Frangi et al. [Frangi 2002], Mitchell et al. [Mitchell 2002], and Lotjonen et al. [Lotjonen 2004] were the first to develop human ventricular statistical shape models. More recently Ordas et al. [Ordas 2007] developed a computational atlas of the entire heart using registration-based techniques. Perperidis et al. [Perperidis 1995, Perperidis 2005] and Hoogendoorn et al. [Hoogendoorn 2007] proposed 4D spatio-temporal human cardiac probability atlases from (MRI), while Beg et al. [Beg 2004] developed a large deformation diffeomorphic mapping (LDDM) for construction of cardiac statistical atlases. As an extension to Beg's work, Helm et al. [Helm 2006] employed LDMM to achieve inter-subject registration to a reference anatomical template to compare cardiac geometric variability using Principle Component Analysis (PCA) from diffusion tensor MRI in normal and failing human hearts.

Manual and semi-automated segmentation and registration approaches

Critical to successful constructions of atlases and to the transformation of constructed surface models to the finite element models (for subsequent computational work of mechanical function), are efficient and accurate segmentation and registration techniques (Figures 13, 14). Using recently developed techniques in our group [Perperidis 2011], a segmented (template) reference MRI sequence is selected from the mouse database consisting of imaged anatomic structures (left and right ventricular myocardium, left and right ventricular blood pools, and papillary muscles) as representative sets of typical anatomic objects of interest. This template is subsequently used to register population images via global and local non-rigid transformations. Although such high-dimensional transformation differs from established one-to-one (invertible) diffeomorphic transformations [Helm 2006], its performance is comparable in accuracy, precision, simplicity, and computational intensity, as recently reported by a multi-center quantitative ranking of 14 different non-linear deformation algorithms [Klein 2009].

Figure 13 show examples of manual, user-based spline segmentation and subsequent correction for left and right ventricular feature extraction, as discussed previously [Perperidis 2011]. Implementation of a global and local registration scheme is also diagrammatically summarized in Figure 14 [Perperidis 2011].

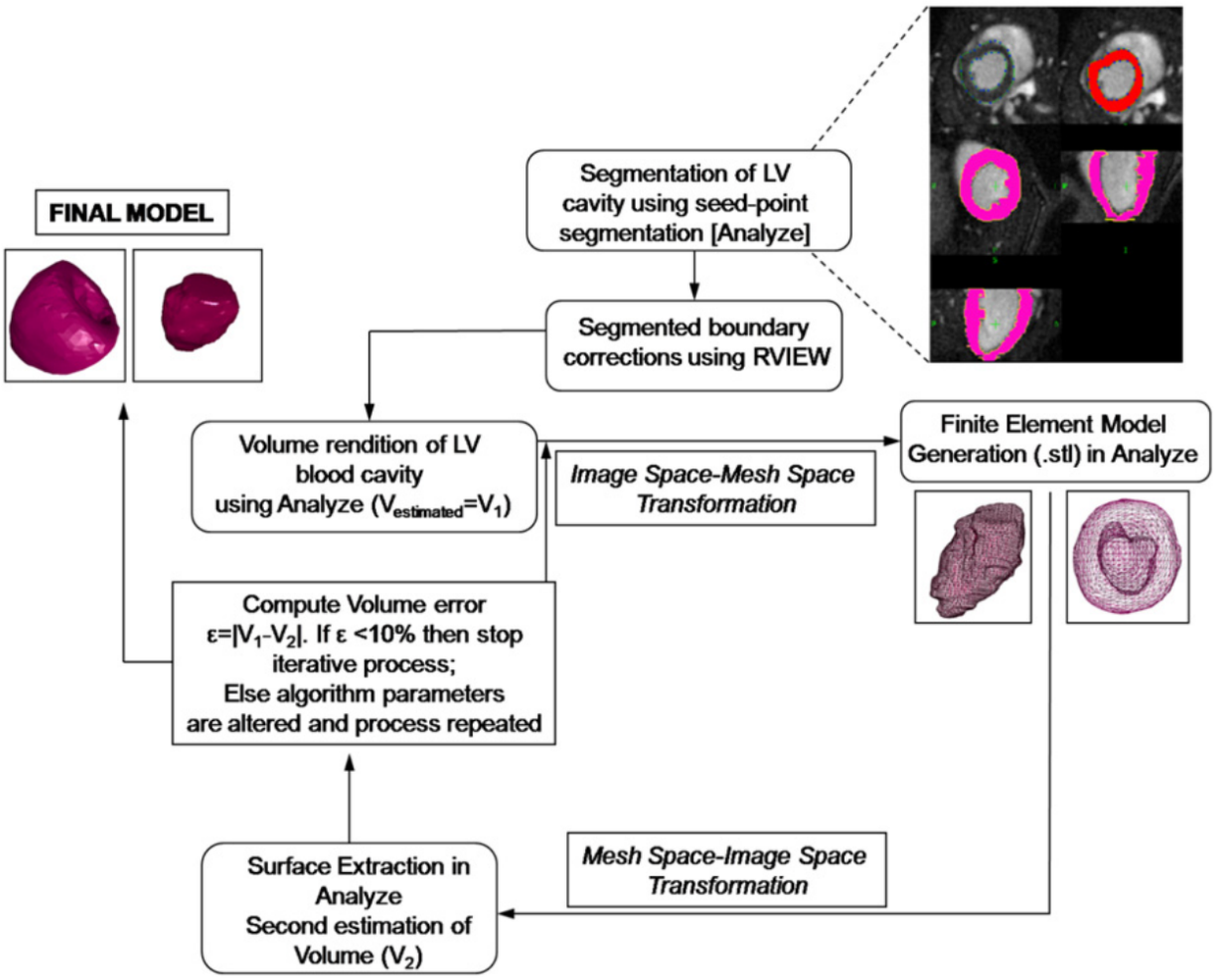

Figure 13. Flow diagrammatical representation of the empirical optimization process for generation of quantitatively accurate finite element models of the murine myocardium. [Reproduced from Constantinides et al. [Constantinides_SBI_2010] with permission from IEEE]. Insert (top right): (top row) Seed-point segmentation and binary mask construction in short axis MRI; (middle and bottom rows) RView 3D binary mask correction. [This work originally appeared in Constantinides et al. [Constantinides 2010] and Perperidis et al. [Perperidis et al. 2011], and was published in Computerized Medical Graphics and the IEEE Proceedings of the International Society of Biomedical Imaging; Reproduced with the permission of Elsevier and IEEE].

Manual, image-based techniques seem to provide the best avenue for segmentation (despite their inherent intra- and inter-observer variability inaccuracies).

Certainly, atlas-based approaches are envisaged to be of tremendous benefit and value for cardiac phenotyping characterization in the upcoming years, aiding spatial mapping of gene expression using novel cellular and sub-cellular probes and markers, understanding embryogenesis and development, accurately mapping strain-, age-, and sex-based morphological dependencies, quantifying patterns of motional variability, and efficiently screening cardiac functional changes based on semi-automatic template segmentation techniques for efficient estimation of hemodynamic indices of function, and high throughput phenotypic screening.

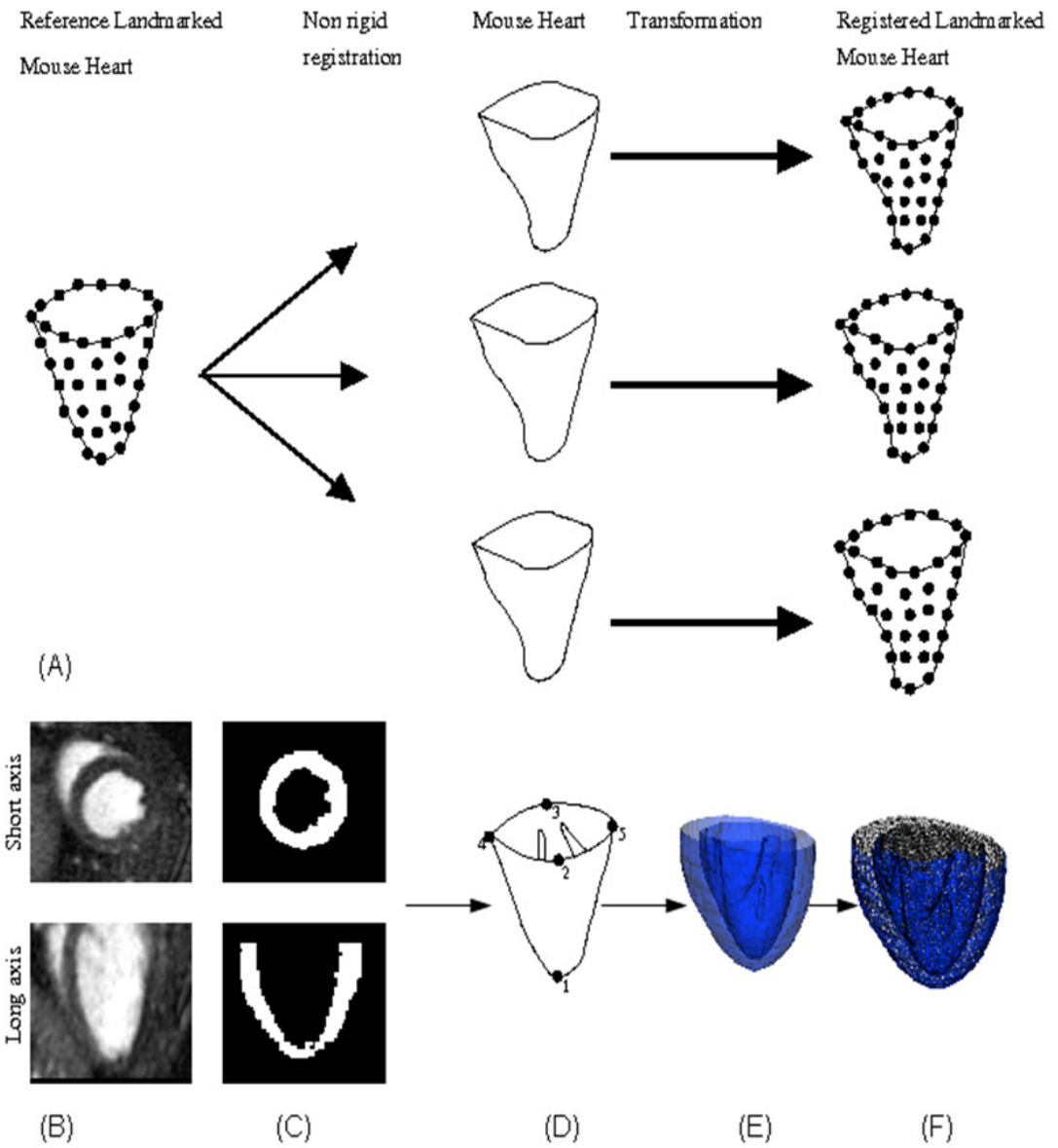

Figure 14. Graphical representation of land-marking as an initial step to image registration. The landmarks are propagated from a reference landmarked template heart model to each remaining mouse heart of each cohort. (B) Typical mid-short and long-axis images from a mouse heart; (C) RView corrected binary masks; (D) Example of five-point landmarked mesh for global registration; (E) 3D epicardial/endocardial reference surface model rendition used for local registration, and (F) construction of the three-dimensional (3D) mesh volumetric dataset using the marching cubes algorithm. [This work originally appeared in Perperidis et al. (Perperidis et al. 2011), published in Computerized Medical Graphics; Reproduced with the permission of Elsevier].

Despite its potential usefulness, the major limitations of such a technique is associated with the significant image post-processing, the need for accurate registration methods (often a challenging task for cardiac datasets), the inherent assumptions associated with the normality of distribution of independent datasets, and confounding factors on attempts to analyze motion and variability (often as a direct modulation of anesthesia effects).

3.4.2. Interstrain comparisons of global cardiac function

Apart from early attempts [Wiesmann 2000], little work has been published on interstrain comparisons of global cardiac functional differences in various mouse strains [Constantinides_SBI 2010, Bucholz 2010]. Instead, studies of cardiac dysfunction have often included quantitative comparisons with normal control or sham mice [Zhang 2008]. Interstrain variability on cardiac function exists in different mouse strains, which may be dependent or independent of strain, but there are certainly developmental factors and other factors that ought to be investigated. Reported results must thus be carefully considered for age, weight, sex, and genetic background. In recent findings from our group (Figure 15) no significant variations in cardiac function were observed from age-, sex-matched (male), normal C57BL/6J and DBA/2J mice. Image-derived hemodynamic indices of function reported in Figure 16 exemplify similar cardiac functional responses from both the right and left ventricular cavities, in agreement with prior reports [Zhang 2008].

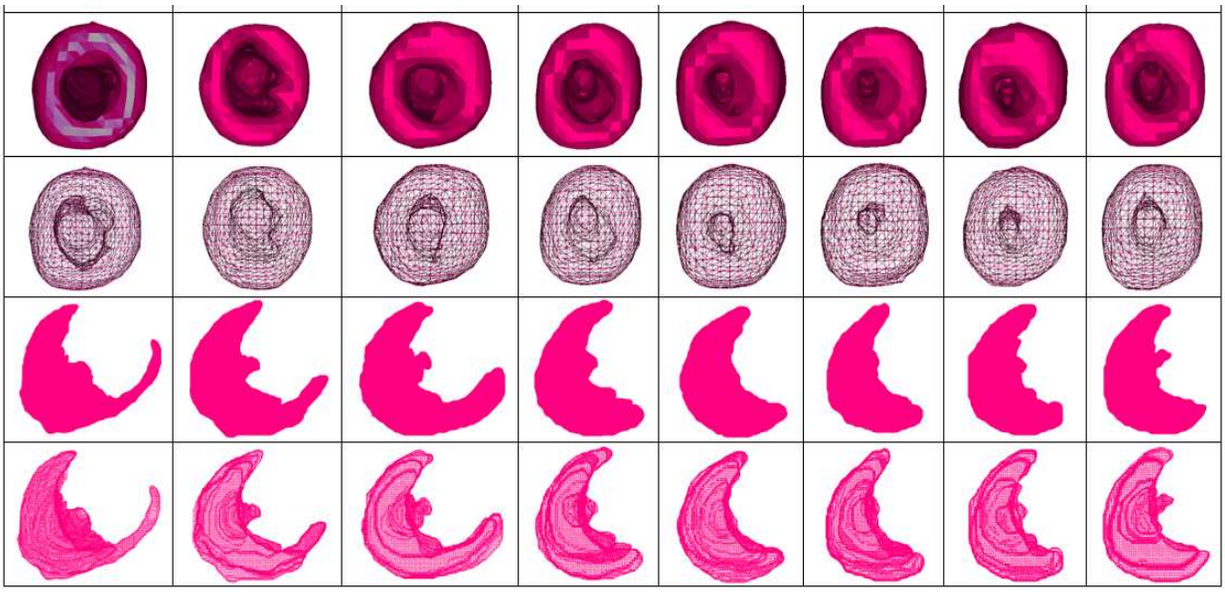

Figure 15. Typical (top two rows) LV surface and finite element, and (bottom two rows) corresponding RV representation of the 4D dynamic surface and finite element model of DBA/2J mice through eight cardiac phases over the entire cardiac cycle.

3.4.2.1. Quantification of regional cardiac function - Comparison of mouse and human

Despite the usefulness of global cardiac index comparisons, the value and importance of regional cardiac functional analyses in disease is paramount. Further to the use of tagging [Liu 2006] and DENSE [Gilson 2005, Zhong 2010] as non-invasive techniques for assessment of regional cardiac displacement and strain in mice, similar patterns of motional responses were observed in mice and humans with noted finite, but distinct, differences. Particularly, Gilson [Gilson 2005] reports basal displacement but almost no apical displacements in the mouse during the cardiac cycle, in comparison to both apical and basal motion in humans [Moore 2000]. Furthermore, circumferential and radial displacements seem to scale proportionally with values previously reported in humans [Constantinides_Phantom 2012].

Finite differences may exist but careful consideration of other factors (such as age, sex, or anesthesia effects) must also be considered in such analyses.

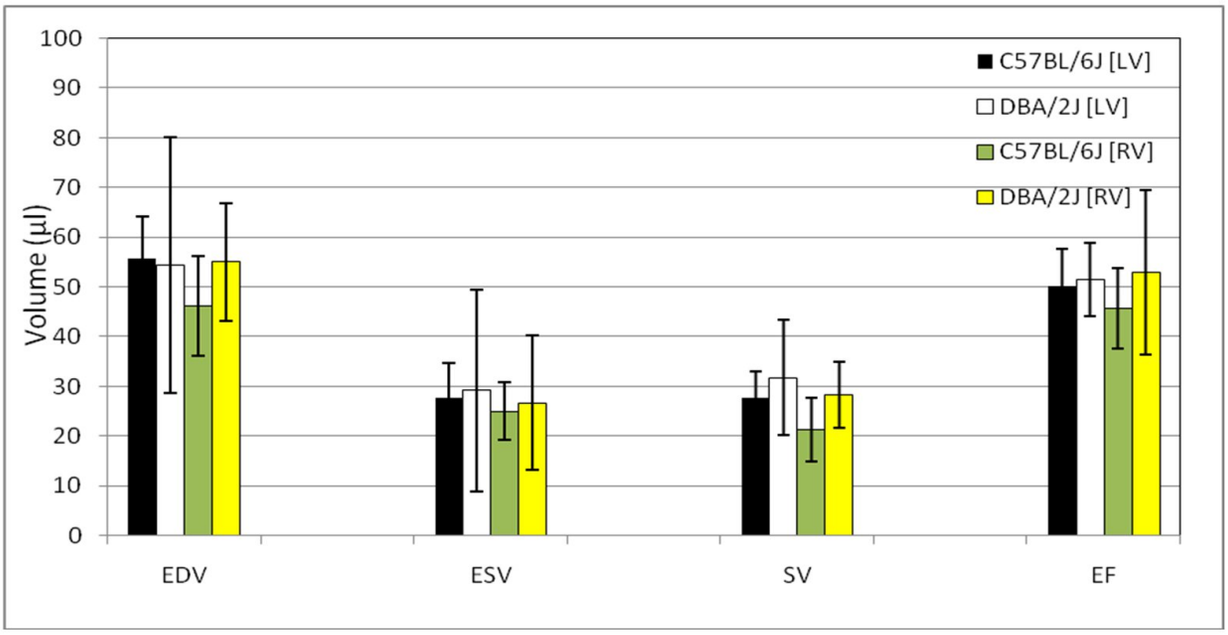

Figure 16. Interstrain hemodynamic (EDV, ESV, SV, EF) index comparisons for left (LV) and right (RV) ventricular performance in male C57BL/6J (n=5) and DBA/2J mice (n=5) based on MRI.

Apart from tissue displacement encoding techniques other motion tracking [Osman 1999], velocity [Streif 2003], and acceleration techniques [Staehle 2011] have been reported.

Despite the importance of all such techniques they nevertheless necessitate access to dedicated high-field MRI scanners and invariably require development, or use, of complex algorithms and reconstruction software. An easier methodology to assess regional cardiac function for comparison with humans was recently reported by Constantinides et al. [Constantinides_ISMRM 2011] with the use of dedicated software (Figure 17) based on segmented epicardial and endocardial boundaries, according to:

$$Wall\,Motion = ED_{epicardial\_wall\_diameter} - ES_{epicardial\_wall\_diameter} \tag{1}$$

$$Wall\,Thickening = 100.\frac{\left(ES_{wall\_thickness} - ED_{wall\_thickness}\right)}{ED_{wall\_thickness}} \tag{2}$$

$$rEF = 100.\frac{\left(ED_{endocardial\_diameter}{}^{2} - ES_{endocardial\_diameter}{}^{2}\right)}{ED_{endocardial\_diameter}{}^{2}} \tag{3}$$

Based on such analyses, bullseye-plots of regional cardiac function were generated in 17-sector representations of the murine and human hearts (from independent studies in two separate Institutions) showing similar patterns in transmural variations in wall motion and thickness, and regional ejection fraction (Figure 18) in mouse and man. Such spatial patterns observed for mouse and human (in agreement with prior tagging work [Moore 2000]) are supported by two-tailed paired t-tests indicating absence of statistical significant differences in the mean values of wall thickness ($p=0.07$), wall motion ($p=0.051$), or regional EF ($p=0.065$) at the 1% significance. Repeated measures ANOVA indicated significant differences in regional mouse and human for wall thickness ($p=0.002$) and regional EF ($p<0.0001$) and insignificant differences for wall motion ($p=0.016$) at the 1% significance. However, despite the similarity in such patterns, quantification of global and regional functional indices (Table 2) shows distinct, finite differences, in agreement with prior reports. Unknown at this stage is whether such differences can be attributed to species variability or endogenous or exogenous parameter dependencies, as they relate to the conduct of such studies and data analyses, or the modus operandi of the human and murine hearts.

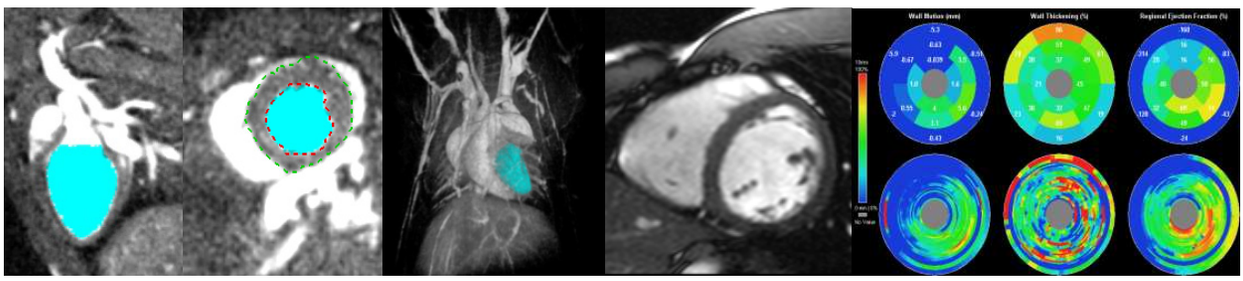

Figure 17. (Left to right) Epicardial and endocardial LV contour definition in mouse long and short - axis MRI, and 3D LV blood cavity segmentation; 3D ventriculogram rendition using Vitrea from murine MRI; short axis human MRI, and Vitrea reconstruction of wall motion, wall thickening, and regional ejection fraction from a typical mouse dataset.

Therefore, numerous practical benefits are associated with dedicated, state-of-the-art mouse cardiac MR imaging, including the non-invasive nature of the techniques, the inherent capability to map cardiac morphology and function, for both LV and RV chambers, and their motional patterns. High spatial and temporal resolution imaging can thus be achieved, through execution of high-throughput protocols, yielding direct, accurate estimates of global and regional indices of cardiac function, avoiding any assumptions whatsoever or model-based derivation approaches endorsed by other imaging techniques such as ultrasound.

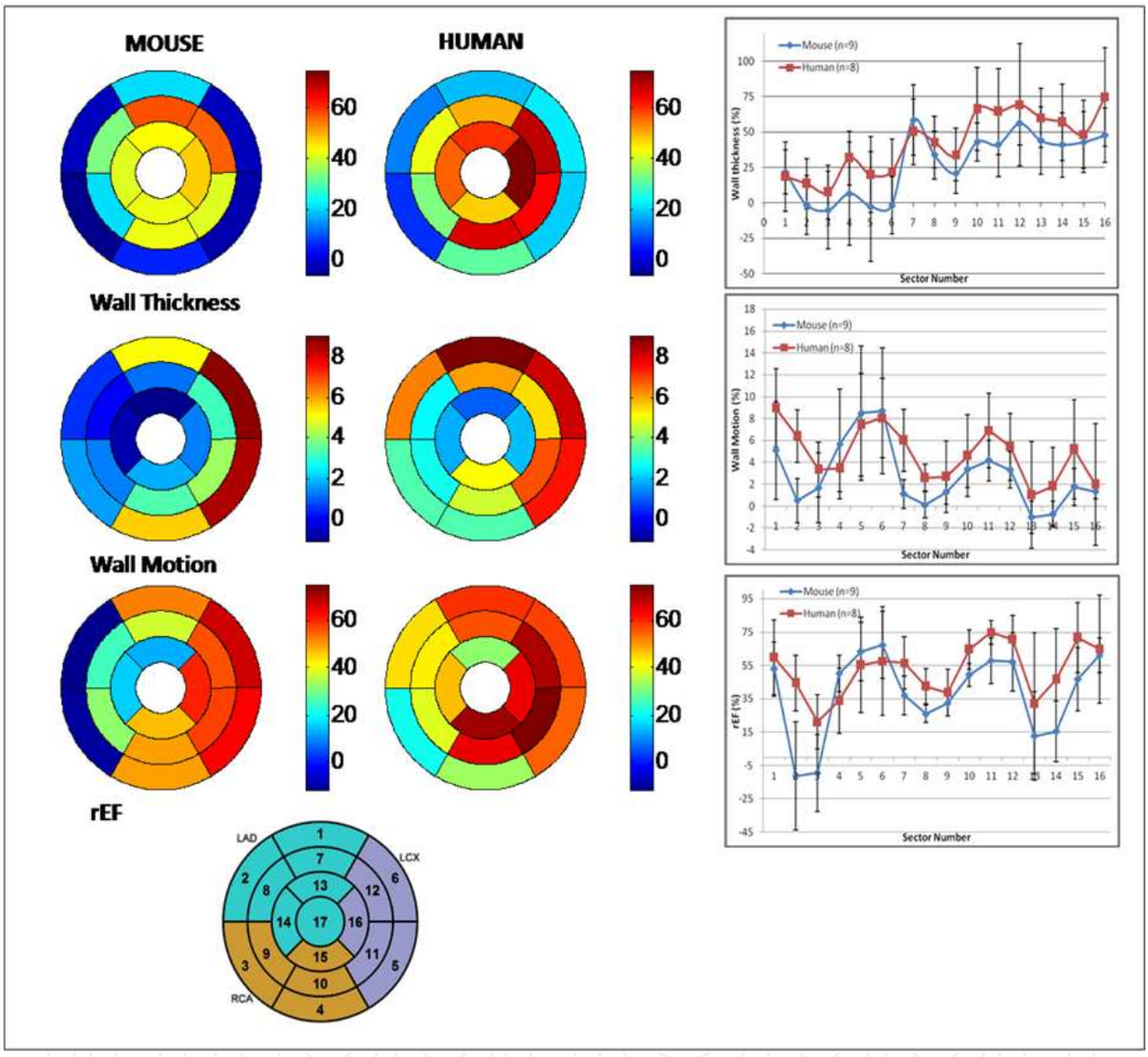

Figure 18. (Left, middle) Regional parameter quantification and comparisons in the mouse and the human using VITREA. Mean bullseye plots for wall motion, wall thickening, and regional ejection fraction for C57BL/6J mice (n=9) and human (n=8) datasets over the entire cardiac cycle. Schematic diagram of sectoral representation of the heart according to AHA guidelines; (right) Regional cardiac performance inter-comparison of mouse and human, including wall thickness, wall motion, and rEF variation in the various sectors of the murine and human hearts (sector 17 is excluded from presented results).

As an extension of the development and use of such techniques (DENSE, tagging, HARP) has been the tremendous value for regional cardiac functional quantification and direct applicability to transgenic mice and in pathological states (myocardial infarction, heart failure).

Such approaches are, however, associated with a number of limitations and drawbacks, including the necessity for use of complex algorithms and laborious data post-processing (tagging, HARP, and DENSE), the inherently low spatial resolution for strain quantification (tagging vs. DENSE), the T_1-tag dependence, the low SNR performance of DENSE (often with a temporal decreasing dependence following ECG-triggering), and the necessity to eliminate the anti-echo and free-induction decay signals in DENSE through proper acquisition adjustments and/or image subtractions.

Cardiac Index	Mouse (n=9)	Human (n=8)
EF	50.7±3.7 %	64.4±2.4 %
EDV	45.4±11.0 μl	117±32.7 ml
ESV	22.5±6.2 μl	46.5±10.3 ml
SV	22.9±5.4 μl	83±15.4 ml
CO	1.4±0.3 ml/min	5.0±0.9 l/min
Myocardial Mass	-	153.1±37.2 g
rEF	38.0±25.0 %	52.2±15.8 %
Wall Thickness	27.9±22.4 %	42.6±21.8 %
Wall Motion	2.8±3.0 %	4.8±2.4 %

Table 2. Summary of mean global and regional cardiac mechanical functional indices (±sd) of murine and human myocardium.

4. Future perspectives

In the new era of molecular imaging, MRI faces major challenges in accomplishing detection of molecular probes with increased sensitivity and specificity, comparable to other diagnostic techniques (such as PET/SPECT). Currently, 10-100 μmolar sensitivity is attained by MRI in contrast to the established nano- and picomolar sensitivity of PET and SPECT. While a new generation of contrast agents is anticipated to extend current limits shedding new light into cellular and molecular mechanisms, current efforts focus primarily on stem cell technology, cellular tracking, and construction of hybrid PET/MRI systems, as discussed below.

4.1. Molecular imaging

Regenerative techniques – Stem cell technology and cellular tracking

Advances in the biology of stem cells have evoked great interest in cell replacement therapies for the regeneration of heart tissue after myocardial infarction. Despite the initial

controversial results from human trials [Rosenzweig 2006] due to the uncertain and unclear long-term fate, target-destination of the injected cells, their engraftment and viability, scientific interest and excitement remains high.

Employing high-resolution MRI in association with metabolism, iron-oxide labeled cells [Stuckey 2006] can be tracked and visualized thereby monitoring their migration patterns and ultimate engraftment fate in tissues of interest.

4.2. Hybrid system imaging

The superb ability of PET to detect ligand-receptor binding at the nano- to picomolar concentrations and the excellent spatial resolution of MR imaging, have stimulated efforts for the construction of hybrid PET/MRI systems. While the first prototype systems have already been completed [Herzog 2010, Pichler 2008], it will be of interest to see if corporate interest will aid establish such hybrid imaging techniques as tools of the arsenal of other diagnostic tools for clinical practice and for basic science research.

5. Conclusion

In the short-lived period of mouse cardiac MRI of the past 15 years, tremendous strides have been made for image-based phenotyping of the cardiovascular system. Such were realized in terms of the scalability of equipment, ease of handling and maintaining animals under proper physiological homeostatic conditions, adaptation of conventional imaging techniques, and inception of new, fast imaging acquisition schemes that have revolutionized cardiac, image-based phenotyping with efficient, high-throughput imaging protocols.

In conclusion, despite the usefulness, practicality, and low costs associated with the study of the mouse, important genetic, developmental, morphological, and cardiovascular system differences exist between mouse and man especially as such are unmasked in pathological conditions or under stress. Physiological results indicate that the optimal ISO anesthetic regimen for mouse studies under anesthesia is approximately 1.5% v/v, yielding stable MAP and HR values comparable to those observed in the animal's conscious state, with a minute-to-minute variability in MAP and HR of ≤11%. Based on such recordings, the optimal FiO_2 appears to be 50%. The additional use of N_2O was associated with higher and more stable values of MAP and HR (at a mixture of 25–50% O_2 and 75–50% N_2O). Arterial pH values are within the physiological range and varied between 7.20 and 7.43. ISO anesthesia at 1.5% v/v is also associated with mild hyperglycemia (+47%) whereas insulin levels remain unaltered. The protocol described for physiological studies of mice under anesthesia has the potential for high reproducibility in diagnostic modalities, including MRI, microCT, ultrasound, and microPET. This regimen can be useful in phenotypic screening and pharmacological studies of cardiac function in mice and can facilitate the transfer of such work to noninvasive imaging platforms, with tremendous potential for both basic science and translational research.

Basic MRI studies of murine global cardiac structure and function under optimal physiological conditions, in combination with PCA and other image processing techniques,

can identify modal components of shape variability and disseminate components of global mechanical motion. Such atlases can be population-based instead of single-subject based and can serve as a powerful reference tool for morphological and functional inter-strain mouse studies, complementary to current ongoing efforts for image-based phenotyping that target the cardiovascular system. Based on constructed morphometric maps and atlases using principal component analysis in C57BL/6J, it is found that in probabilistic atlases, a gradient of probability exists for both strains in longitudinal locations from base to apex. Based on the statistical atlases, differences in size (49.8%), apical direction (15.6%), basal ventricular blood pool size (13.2%), and papillary muscle shape and position (17.2%) account for the most significant modes of shape variability for the left ventricle of the C57BL/6J mice. Correspondingly, for DBA mice, differences in left ventricular size and direction (67.4%), basal size (15.7%), and position of papillary muscles (16.8%) account for significant variability. These data reason in favor of existing variability in the apical location in both strains, a direct consequence of the heart's effort to re-establish the position of the apex in a consistent manner at end-diastole. Additionally, higher variability exists in DBA mice in the location of the papillary muscles, as well as in the epicardial areas of the left ventricle.

On the forefront of direct, high-field acquisitions using RF technologies with mouse cardiac MRI, the commercially available birdcage outperforms cylindrical spiral multi-turn surface coils in relative signal-to-ratio (SNR) by a factor of 3–5 times as assessed by experimental measurements, simulations, and experiments in free space, and under phantom and animal loading conditions. Nevertheless, quantitative comparison of the performance of the two spiral coil geometries in anterior, lateral, inferior, and septal regions of the murine heart yield maximum mean percentage rSNR increases to the order of 27–167% post-mortem (cylindrical compared to flat coil), values that are by far higher than previous designs of surface coils and comparable to receiver phased array performance.

Such hardware improvements, in association with fast radial pulse sequence acquisitions, may also lead to quantification of global and regional functional parameters in various mouse strains. While morphological differences appear only to relate to increased papillary muscle variability in the DBA/2J mice, nevertheless interstrain cardiac hemodynamics, based on dynamic cardiac MRI acquisitions, do not exhibit significant differences for neither the LV nor RV in C57BL/6J or DBA/2J mice. Comparative to previous reports of global functional indices [Bucholz 2010], similar mouse and human results were also observed. The work supports the validity of the hypothesis of functional scaling in mice and humans.

Author details

Christakis Constantinides
Laboratory of Physiology and Biomedical Imaging (LBI),
Department of Mechanical and Manufacturing Engineering, School of Engineering,
University of Cyprus, Nicosia, Cyprus

Acknowledgement

I would like to thank Professors G. A. Johnson, G. Truskey, L. Hedlund, and Dr. E. Bucholz, Mr. G. Cofer, and Mr. J. Cook at Duke University, Drs. R. Balaban and A. Koretsky, and Mr. D. Despres and Dr. M. Lizak at the National Institutes of Health, Prof. D. Rueckert at Imperial College, London, Professor BA Janssen at Maastricht Cardiovascular Institute, and my fellows and students Dr. D. Perperidis, Mr. N. Aristocleous, Mr. R. Mean, Mr. S. Gkagkarelis, and Mr. S. Angeli at the University of Cyprus. I am indebted to the help and support from Remcom Inc. I am also grateful for the availability of the Image Registration Toolkit used under License from IXICO Ltd and to Dr. E. Treiber from Bruker Biospin for the provision of the cardiac MR images.

I would also like to acknowledge grant support from the Research Promotion Foundation (RPF) under grants RPF/TEXNOLOGY/MHXAN/0609(BE)/05, RPF/STOXOS/0302/02, and RPF/PROSVASI/0302/01.

6. References

[1] Aletras A, Ding S, Balaban RS, Wen H. DENSE: Displacement encoding with stimulated echoes in cardiac functional MRI. J. Magnetic Resonance 1999; 137: 247-252.

[2] Ali A, Dale AM, Badea A, Johnson GA. Automated segmentation of neuroanatomical structures in multispectral MR microscopy of the mouse brain. Neuroimage 2005; 27:425–35.

[3] Axel L, Dougherty L. MR Imaging of motion with spatial modulation of magnetization. Radiology 1989; 171(3):841-5.

[4] Badea C, Fubara B, Hedlund L, Johnson G. 4D micro-CT of the mouse heart. Molecular Imaging 2005; 4(2):110-116.

[5] Balaban RS, Hampshire VA. Challenges in Small Animal Noninvasive Imaging. ILAR 2001; 42(3):248-262.

[6] Barbee RW, Perry BD, Re RN, Murgo TP. Microsphere and dilution techniques for the determination of blood flows and volumes in conscious mice. Am J Physiol Regulatory Integr Comp Physiol 1992; 263:R728-R733.

[7] Barbee RW, Perry BD, Re RN, Murgo JP, Field LJ. Hemodynamics in Transgenic Mice with Overexpression of Atrial Natriuretic Factor. Circ. Res. 1994; 74:747-751.

[8] Beg MF, Helm PA, McVeigh E, Miller MI, Winslow RL. Computational cardiac anatomy using MRI. Magn Reson Med 2004; 52:1167–74.

[9] Bernston GC, Bigger JT Jr, Eckberg DL, Grossman P, Kaufmann PG, Malik M, Nagaraja HN, Parges SW, Paul JP, Stone PH, Van Der Molen MW. Heart rate variability: origins, methods, and interpretive caveats. *Psychophysiol*. , 1997; 34:623- 648.

[10] Berr SS, Roy RJ, French BA, Yang Z, Gilson W, Kramer CM, Epstein FH. Black blood gradient echo Cine magnetic resonance imaging of the mouse heart. Magn Reson in Med 2005; 53:1074-1079.

[11] Bishop J, Feintuch A, Bock NA, Nieman B, Dazai J, Davidson L, Henkelman RM. Retrospective gating for mouse cardiac MRI. Magn Reson in Med 2006; 55(3):472-477.

[12] Blank S, Chen V, Hamilton N, Salerno T, Ianuzzo C. Biochemical characteristics of mammalian myocardial. J Mol Cell Cardiol 1989; 21:367-373.

[13] Bock NA, Konyer NB, Henkelman RM. Multiple-mouse MRI. Magn Reson in Med 2003; 49(1):158-167.

[14] Bovens SM, te Boekhorst BC, den Ouden K, van de Kolk KW, Nauerth A, Nederhoff MG, Pasterkamp G, ten Hove M, van Echteld CJ. Evaluation of infracted murine cardiac function: comparison of prospectively triggered with self-gated MRI. NMR in Biomedicine 2011; 24(3):307-315.

[15] Brede M, Hadamek K, Meinel L, Wiesmann F, Peters J, Engelhardt S, Simm A, Haase A, Lohse MJ, Hein L. Vascular hypertrophy and increased P70S6 kinase in mice lacking the angiotensin II AT(2) receptor. Circulation 2001; 104(31):2602:2607.

[16] Brunson DB. Pharmacology of inhalation anesthetics (Chapter 2). In: Fish RE, Brown MJ, Danneman PJ, Karas AZ (eds.) Anesthesia and Analgesia in Laboratory Animals. 2nd ed. London: Academic Press. 2008; p29-41.

[17] Bucholz E, Ghaghada K, Qi Y, Mukundan S, Johnson GA. Four-dimensional MR microscopy of the mouse heart using radial acquisition and liposomal gadolinium contrast agent. Magn Reson Med 2008; 60:111–8.

[18] Bucholz E, Ghaghada K, Qi Y, Mukundan S, Rockman H, Johnson GA. Cardiovascular phenotyping of the mouse heart using a 4D radial acquisition and liposomal Gd-DTPA-BMA. Magn Reson in Med 2010; 63(4):979-97.

[19] Carr HY. Steady-State Free Precession in Nuclear Magnetic Resonance. Physical Review 1958; 112:1693-1701.

[20] Cassidy PJ, Schneider JE, Grieve SM. Lygate C, Neubauer S, Clarke K. Assessment of Motion Gating Strategies for Mouse Magnetic Resonance at High Magnetic Fields. Journal of Magnetic Resonance Imaging 2004; 19:229–237.

[21] Chacko VP, Aresta F, Chacko SM, Weiss RG. MRI/MRS assessment of in vivo murinecardiac metabolism, morphology, and function at physiological heart rates. Am J Physiol Heart Circ Physiol 2000; 279(5):H2218-H2224.

[22] Chien KR. To Cre or not to Cre: the next generation of mouse models of human cardiac diseases. Circ Res 2000; 88:546–9.

[23] Cholewa BC, Mattson DL. Role of the renin-angiotensin system during alterations of sodium intake in conscious mice. Am J Physiol Regul Integr Comp Physiol 2001; 281:R987-R933.

[24] Chuang JS, Zemlijic-Harpf A, Ross RS, Frank LR, McCulloch AD, Omens JH. Determination of three-dimensional ventricular strain distributions in gener-targeted mice using tagged MRI. Magnetic Reson Med 2010; 64(5):1281-8.

[25] Collins FS, Green ED, Guttmacher AE, Guyer MS. A vision for the future of genomics research: A blueprint for the genomic era. Nature 2003; 422(6934):835-847.

[26] Constantinides C, Mean R, Janssen BJ. Effects of Isoflurane Anesthesia on the Cardiovascular Function of the C57BL/6 Mouse. ILAR 2011; 52:e21-e31.

[27] Constantinides C, Angeli S, Mean R. Changes in Murine Cardiac Ionotropy and Hemodynamics following Manganese administration under isoflurane anesthesia. Annals in Biomedical Engineering 2011; 39(11):2706-2720; DOI: 10.1007/s10439-011-0367-5 (accessed August 5, 2011).

[28] Constantinides C, Angeli S, Gkagarelis S, Cofer G. Intercomparison of performance of RF Coil Geometries for High Field Mouse Cardiac MRI. Concepts of Magnetic Resonance Part A 2011; 38A(5):236-252. DOI 10.1002/cmr.a.20225 (accessed 4 August 2011).

[29] Constantinides C, Mean R, Janssen BA. Heart rate and blood pressure variability effects as a result of oxygen and nitrous oxide administration in the anesthetized Mouse 2010: 32nd Annual International Conference of the IEEE Engineering in Medicine and Biology Society (IEEE-EMBS) 'Merging Medical Humanism and Technology', August 2010, 2010, Buenos Aires, Argentina.

[30] Constantinides C, Aristocleous A, Johnson A, Perperidis D. Static and Dynamic Cardiac modeling: initial strides and results towards a quantitatively accurate mechanical heart model 2009: Proceedings of the IEEE Society on Biomedical Imaging (SBI), Rotterdam, The Netherlands, February 2009.

[31] Constantinides C, Angeli A, Mean R. Murine cardiac catheterizations and hemodynamics: On the issue of parallel conductance, IEEE Transactions of Biomedical Engineering 2011; 58(11), 3260-3268.

[32] Constantinides C, Angeli S, Kossivas F, Ktorides P. Underestimation of cardiac hemodynamics using invasive catheters: errors, limitations, and remedies. Cardiovascular Engineering Technology 2012; 3(2):179-193; DOI: 10.1007/s13239-012-0084-8 (accessed June 2012).

[33] Constantinides C, Nearchou D, Constantinou C, Ktorides P, Gravett R, Tzagarakis V. A Novel Cardiac Phantom to Study Murine and Human Cardiac Motion and Function using MRI 2011: Proceedings of the International Society of Magnetic Resonance in Medicine, Montreal, Canada 2011.

[34] Constantinides C, Zhong X, Tzangarakis G, Cofer G, Gravett R. A Computer-Controlled Cardiac Phantom to Emulate Human and Murine Motion using DENSE MRI. Submitted, June 2012.

[35] Dobson GP, Headrick JP. Bioenergetic scaling: Metabolic design and body-size constraints in mammals. Proc. Natl. Acad. Sci. USA 1995; 92:7317-7321.

[36] Doevendans PA, Daemen MJ, de Muinck ED, Smits JF. Cardiovascular phenotyping in mice. Cardiovascular Research 1998; 39:34–49.

[37] Dawson D, Lygate C, Saunders J, Schneider JE, Ye X, Hulbert K, Noble JA, Neubauer S. Quantitative 3-Dimensional Echocardiography for accurate and rapid cardiac phenotype characterization in mice. Circulation 2004; 110:1632-1637.

[38] Ehmke H. Mouse gene targeting in cardiovascular physiology. Am J Physiol Regul Integr Comp Physiol 2003; 284: R28–R30.

[39] Engel D, Peshock R, Armstong RC, Sivasubramanian N, Mann DL. Cardiac myocyte apoptosis provokes adverse cardiac remodeling in transgenic mice with targeted TNF overexpression. Am J Physiol Heart Circ Physiol 2004; 287(3):H1303-H1311.

[40] Epstein FH, Yang Z, Gilson WD, Berr SS, Kramer CM, French BA. MR tagging early after myocardial infarction in mice demonstrates contractile dysfunction in adjacent and remote regions. Magn Reson in Med 2002; 48(2):399-403.

[41] Epstein FH. MR in mouse models of cardiac disease. NMR Biomed 2007; 20(3):238–55.

[42] Feng MG, Dukaez SAW, Kline RL. Selective effect of tempol on renal medullary hemodynamics in spontaneously hypertensive rats. Am J Physiol Regul Integr Comp Physiol 2001; 281:R1420-R1425.

[43] Frahm J, Hanicke W, Merboldt KD. Transverse coherence in rapid FLASH NMR Imaging. Journal of Magnetic Resonance 1987;72:307-314.

[44] Frangi A, Rueckert D, Schnabel J, Niessen W. Automatic construction of multiple-object three-dimensional statistical shape models: applications to cardiac modelling. IEEE Trans Med Imag 2002; 21(9):1151–66.

[45] Franco F, Dubois SK, Peshock RM, Shohet RV. Magnetic resonance imaging accurately estimates LV mass in a transgenic mouse model of cardiac hypertrophy. Am J Physiol 1998; 274:H679-H683.

[46] Franco F, Thomas GD, Giroir B, Bryant D, Bullock MC, Chwialkowski MC, Victor RF, Peshock RM. Magnetic resonance imaging and invasive evaluation of heart failure in transgenic mice with myocardial expression of tumor necrosis factor-alpha. Circulation 1999; 99(3):448-454.

[47] Frydrychowicz A, Spindler M, Rommel E, Erti G, Haase A, Neubauer S, Wiesmann F. Functional assessment of isolated right heart failure by high resolution in-vivo cardiovascular magnetic resonance in mice. Journal of Cardiovascular Magnetic Resonance 2007; 9:623-627.

[48] Gehrmann, Hammer PE, Maguire CT, Wakimoto H, Triedman JK, Berul CI. Phenotypic screening for heart rate variability in the mouse. Am. J. Physiol. Heart Circ Physiol 2000; 279:H733-H740.

[49] Georgakopoulos D, Mitzner W, Chen CH, Byrne BJ, Millar HD, Hare JM, and Kass DA, "In vivo murine left ventricular pressure–volume relations by miniaturized conductance micromanometry," Amer. J. Physiol. Heart Circ. Physiol 1998; 274(43): H1416–H1422.

[50] Gilson WD, Yang Z, French BA, Epstein FH. Measurement of myocardial mechanics in mice before and after infarction using multislice displacement-encoded MRI with 3D motion encoding. Am J Physiol Heart Circ Physiol 2005; 288:H1491-H1497.

[51] Gregory SG, Sekhon M, Schein J, Zhao S, Osoegawak K, Scott CE, Evans RS, Burridge PW, Cox TV, Fox CA, Hutton RD, Mullenger IR, Phillips KJ, Smith J, Stalker J, Threadgold GJ, Birney E, Wylie K, Chinwalla A, Wallis J, Hillier L, Carter J, Gaige T, Jaeger S, Kremitzki C, Layman D, Maas J, McGrane R, Mead K, Walker R,

Jones S, Smith M, Asano J, Bosdet I, Chan S, Chittaranjan S, Chiu R, Fjell C, Fuhrmann D, Girn N, Gray C, Guin R, Hsiao L, Krzywinski M, Kutsche R, Sen Lee S, Mathewson C, McLeavy C, Messervier S, Ness S, Pandoh P, Prabhu A-L, Saeedi P, Smailus D, Spence L, Stott J, Taylor S, Terpstra W, Tsai M, Vardy J, Wye N, Yang G, Shatsman S, Ayodeji B, Geer K, Tsegaye G, Shvartsbeyn A, Gebregeorgis E, Krol M, Russell D, Overton L, Malek JA, Holmes M, Heaney M, Shetty J, Feldblyum T, Nierman WC, Catanesek JJ, Hubbard T, Waterston RH, Rogers J, de Jongk PJ, Fraser CM, Marra M, McPherson JD, Bentley DR. A Physical Map of the Mouse Genome. Nature 2002; 418:743-750.

[52] Haase A, Frahm J, Matthaei D, Hanicke W, Merboldt KD. FLASH imaging rapid NMR imaging using low flip-angle pulses. Journal of Magnetic Resonance 1986; 67(2):258-266.

[53] Hart CYT, Burnett JC, Redfield MM. Effects of avertin versus xylazine-ketamine anesthesia on cardiac function in normal mice. Am. J. Physiol. Heart Circ Physiol. 2001; 281:H1938-H1945.

[54] Hedlund LW, Gluckman TL. Basics of Small Animal Handling for In Vivo Imaging (Chapter 24). In: Pomper M, Gelovani J, (eds.) Molecular Imaging in Oncology. First Edition, INFRMAN-HC; 2008; p377-390.

[55] Heijman E, Strijkers GJ, Habets J, Janssen B, Nicolay K. Magnetic resonance imaging of regional cardiac function in the mouse. MAGMA 2004; 17: 170–178.

[56] Heijman E. Mouse Cardiac MRI. Doctoral Thesis. University of Eindhoven, The Netherlands; 2008.

[57] Helm PA, Younes L, Beg MF, Ennis DB, Leclercq C, Faris OP, et al. Evidence of structural remodelling in the dyssynchronous failing heart. Circ Res 2006; 98:125–32.

[58] Henkelman RM. Systems biology through mouse imaging centers: experience and new directions. Annu Rev Biomed Eng 2010; 12:143–66.

[59] Henson RE, Song SK, Pastorek JS, Ackerman JJ, Lorenz CH. Left ventricular torsion is equal in mice and humans. Am J Physiolo Heart Circ Physiol 2000; 278(4):H1117-H1123.

[60] Herzog H,Pietrzyk U, Shah NJ, Ziemons K. The current state, challenges and perspectives of MR-PET. NeuroImage 2010; 49(3):2072-82.

[61] Hildebrandt IJ, Su H, Weber WA. Anesthesia and other considerations for in vivo imaging of small animals. ILAR , 2008; 49(1): 17-26.

[62] Hiba B, Richard N, Thibault H, Janier M. Cardiac and respiratory self-gated Cine MRI in the mouse: comparison between radial and rectilinear techniques at 7T. Magn Reson in Med 2007; 58:745-753.

[63] Hinshaw WS. Image formation by nuclear magnetic resonance: The sensitive point method. Journal of Applied Physics 1976; 8:3709-3721.

[64] Hoit BD. New Approaches to Phenotypic Analysis in Adult Mice. J. Mol. Cell Cardiol. 2001; 33:27-35.

[65] Hoit BD. Murine physiology: measuring the phenotype. *J. Mol. Cell. Cardiol.* 2004; 37:377-387.

[66] Hoogendoorn C, Sukno FM, Ordas S, Frangi AF. Bilinear models for spatiotemporal point distribution analysis: application to extrapolation of whole cardiac dynamics 2007: Proceedings of mathematical methods in biomedical image analysis. Rio de Janeiro, Brazil: IEEE Computer Society Press, p 1–8, 2007.

[67] James JF, Hewett TE, Robbins J. Cardiac Physiology in Transgenic Mice. *Circulation Research* 1998; 82:407-415.

[68] Janssen BJ, Leenders PJ, Smits JF. Short-term and long-term blood pressure and heart rate variability in the mouse. *Am. J. Physiol. Reg. Integr. Comp. Physiol.* 2000; 278(1): R215-R225.

[69] Janssen B, Smits JFM. Autonomic control of blood pressure in mice: basic physiology and effects of genetic modification. *Am. J. Physiol. Reg. Integr. Comp. Physiol.* 2002; 282:R1545-R1564.

[70] Janssen BJA, Celle TD, Debets J, Brouns A, Callahan M, Smith T. Effects of anesthetics on systemic hemodynamics in mice. Am J Physiol Heart Circ Physiol 2004; 287:H1618-H1624.

[71] Johnson GA, Cofer GP, Gewalt SL, Hedlund LW. Morphologic Phenotyping with MR Microscopy: The Visible Mouse. Radiology 2002; 222:789-793.

[72] Kass DA, Hare JM, Georgakopoulos D. Murine Cardiac Function: A Cautionary Tail. Circulation Research 1998; 82:519-522.

[73] Klein A, Andersson J, Ardekani BA, Ashburner J, Avants B, Chiang MC, et al. Evaluation of 14 nonlinear deformation algorithms applied to human brain MRI registration. Neuroimage 2009; 46:786–802.

[74] Kober F, Iltis I, Cozzone PJ, Bernard M. Myocardial Blood Flow Mapping in Mice Using High Resolution Spin Labeling Magnetic Resonance Imaging: Influence of Ketamine/Xylazine and Isoflurane Anesthesia. Magn. Reson. in Med. 2005; 553:601-606.

[75] Kovacs H, Moskau D, Sraul M. Cryogenically cooled probes: a leap in NMR technology. Magnetic Resonance Spectroscopy 2005; 46:131-255.

[76] Kuijer JPA, Jansen E, Marcus JT, van Rossum AC, Heethaar RM. Improved Harmonic Phase Myocardial Strain Maps. Magnetic Resonance in Medicine 2001; 46:993–999.

[77] Lauterbur PC. Image formation by induced local interactions: examples employing nuclear magnetic resonance. Nature 1973; 242:190-191.

[78] Liu W, Ashford MW, Chen J, Watkins MP, Williams TA, Wickline SA, Yu X. MR tagging demonstrates quantitative differences in regional ventricular wall motion in mice, rats, and men. Am J Physiol Heart Circ Physiol 2006; 291: H2515–H2521.

[79] Lotjonen J, Kivisto S, Koikkalainen J, Smutek D, Lauerma K. Statistical shape model of atria, ventricles and epicardium from short- and long-axis MR images. Med Image Anal 2004; 8:371–86.

[80] Ma X, Abboud FM, Chapleau MW. Analysis of afferent, central, and efferent components of the baroreceptor reflex in mice. Am J Physiol Regul Integr Comp Physiol 2002; 283:R1033-R1040.

[81] Manning WJ, Wei JY, Fossel ET, Burnstein D. Measurement of left ventricular mass in rats using electrocardiogram-gated magnetic resonance imaging. Am J Physiol 1990; 258:H1181-H1186.

[82] Markiewicz FX, Zamora M, Karczmar GS, Roman BB. Comparison and evaluation of mouse cardiac MRI acquired with open birdcage, single loop surface, and volume birdcage coils. Phys Med Biol 2006; 51(24):N451-9.

[83] Maze M, Daunt DA, Salonen M. Current Research in Anesthesia and Trends in Clinical Applications (Chapter 17): In: Fish RE, Brown MJ, Danneman PJ, Karas AZ (eds.) Anesthesia and Analgesia in Laboratory Animals. 2nd ed. London: Academic Press 2008; p387-408.

[84] MacGowan GA, Du C, Cowan DB, Stamm C, McGowan FX, Solaro RJ, Koretsky AP, Del Nido PJ. Ischemic Dysfunction in transgenic mice expressing troponin I lacking protein kinase C phosphorylation sites. Am. J. Physiol. Heart Circ. Physiol 2001; 280:H835-H843.

[85] McLean M, Prothero J. Determination of relative fiber orientation in heart muscle: methodological problems. Anat Rec 1992; 232:459-465.

[86] Milano CA, Allen LF, Rockman HA, Dolber PC, McMinn TR, Chien KR, Johnson TD, Bond RA, Lefkowitz RJ. Enhanced Myocardial Function in Transgenic Mice Overexpressing the beta-Adrenergic Receptor. Science 1994; 264:5158:582-586.

[87] Moore CC, Lugo-Olivieri CH, McVeigh ER, Zerhouni EA. Three-dimensional systolic strain patterns in the normal human left ventricle: characterization with tagged MR Imaging. Radiology 2000; 214(2):453-466.

[88] Mitchell S, Bosche J, Lelieveldt B, van der Geest R, Reiber J, Sonka M. 3-D active appearance models: segmentation of cardiac MR and ultrasound images. IEEE Trans Med Imag 2002; 21(9):1167–78.

[89] Nahrendorf M, Wiesmann F, Hiller KH, Han H, Hu K, Waller C, Ruff J, Haase A, Ertl G, Bauer WR. In vivo assessment of cardiac remodeling after myocardial infarction in rats by cine-magnetic resonance imaging. J. Cardiovascular Magn Reson 2000; 2(3):171-180.

[90] Ng L, Lau C, Sunkin SM, Bernard A, Chakravarty MM, Lein ES, Jones AR, Hawrylycz M. Surface-based mapping of gene expression and probabilistic expression maps in the mouse cortex. Methods 2010; 50:55-62.

[91] Nielsen KS, Larimer JL. Oxygen Dissociation Curves of Mammalian Blood in Relation to Body Size. Am. J. Physiol. 1958; 195(2):424-428.

[92] Ohnishi TS, Pressman GS, Price HL. A possible mechanism of anesthetic-induced myocardial depression. Biochemical and Biophysical Research Communications 1974; 57(1):316-322.

[93] Olivetti G, Lagstra C, Quanini F et al. Capillary growth in anemia-induced ventricular wall remodeling in the rat heart. Circ Res 1989; 65:1182-1192.

[94] Ordas S, Oubel E, Sebastian R, Frangi AF. Computational anatomy atlas of the heart. In: International symposium on image and signal processing and analysis (ISPA), 2007; 338–42.

[95] Osman NF, Kerwin WS, McVeigh ER, Jerry L. Prince JL. Cardiac Motion Tracking Using CINE Harmonic Phase (HARP) Magnetic Resonance Imaging. Magn Reson Med. 1999; 42(6): 1048–1060.

[96] Pauling L, Marsh RE. The structure of chlorine hydrate. Proceedings of the National Academy of Sciences 1952; 38:112-118.

[97] Perperidis D, Mohiaddin RH, Rueckert D. Construction of probabilistic and statistical atlases of the cardiac anatomy and function using MR image sequences. Lect Notes Comput Sci, LNCS 1995; 3750:402–10.

[98] Perperidis D, Mohiaddin R, Rueckert D. Spatio-temporal free-form registration of cardiac MR image sequences. Med Image Anal 2005; 9(5):441–56.

[99] Perperidis D, Bucholz E, Johnson GA, Constantinides C. Morphological Studies of the Murine Heart Based on Probabilistic and Statistical Atlases. Computerized Graphics and Medical Imaging 2012; 36(2):119-29. DOI 10.1016/j.compmedimag 2011.07.001 (accessed August 2011).

[100] Phillips D, Covian R, Aponte A, Glancy B, Taylor JF, Chess D, Balaban RS. Regulation of oxidative phosphorylation complex activity: effects of tissue specific metabolic stress within an allometric series and acute changes in workload. Am J Physiol Regul Integr Comp Physiol. 2012; 302(9):R1034-48.

[101] Popovic ZB, Sun JP, Yamada H, Drinko J, Mauer K, Greenberg NL, Cheng Y, Moravec CS, Penn MS, Mazgalev TN, Thomas JD. Differences in left ventricular long-axis function from mice to humans follow allometric scaling to ventricular size. J Physiol 2005; 568.1: 255–265.

[102] Pichler BJ, Judenhofer MS, Wherl HF. PET/MRI hybrid imaging: devices and initial results. European Radiology 2008; 18(6):1077-86.

[103] Price HL, Ohnishi T. Effects of anesthetics on the heart. Federation Proceedings 1980; 39:1575-1579.

[104] Porterfield JE, Kottam ATG, Raghavan K, Escobedo D, Jenkins JT, Larson ER, Trevino RJ, Valvano JW, Pearce JA, Feldman MD. Dynamic correction for parallel conductance, G_p, and gain factor, α, in invasive murine left ventricular volume measurements. J Appl Physiol 2009; 107:1693-1703.

[105] Przylenk K, Groom AC. Microvascular evidence for a transition zone around a chronic myocardial infarct in the rat. Can J Physiol Pharmacol 1983; 61:1516-1522.

[106] Rakusan K, Nagal J. Morphometry of arterioles and capillaries in hearts of senescent mice. Cardiovascular Res 1994; 28(7):969-972.

[107] Ramirez MS, Esparza-Coss E, Bankson JA. Multiple-Mouse MRI with Multiple Arrays of Receive Coils. Magn Reson Med. 2010; 63(3): 803–810.

[108] Rockman HA, Ross RS, Harris AN, Knowlton KU, Steinhelper ME, Field LJ, Ross J, Chien KR. Segregation of atrial-specific and inducible expression of an atrial natriuretic factor transgene in an in vivo murine model of cardiac hypertrophy. Proc Natl Acad Sci USA 1991; 88(18):8277-8281.

[109] Rosenblum W. Regional cerebral blood flow in the anesthetized mouse as measured by local hydrogen clearance. Stroke 1977; 8:103-106.

[110] Rosenzweig A. Cardiac cell therapy – mixed results from mixed cells. The New England Journal of Medicine 2006; 355(12):1274-1277.

[111] Ross AJ, Yang Z, Berr SS, Gilson WD, Petersen WC, Oshinski JN, French BA. Serial MRI evaluation of cardiac structure and function in mice after reperfused myocardial infarction. Magn Reson in Med 2002; 47:1158-1168.

[112] Ruff J, Wiesmann F, Hiller KH, Voll S, von Kienlin M, Bauer WR, Rommel E, Neubauer S, Haase A. Magnetic resonance microimaging for noninvasive quantification of myocardial function and mass in the mouse. Magn Reson Med 1998; 40:43-48.

[113] Ruff J, Wiesmann F, Lanz T, Haase A. Magnetic resonance imaging of coronary arteries and heart valves in a living mouse: techniques and preliminary results. J. Magn Reson 2000; 146(2):290-296.

[114] Sabbah HN, Sharov VG, Lesch M, Goldstein S. Progression of heart failure: a role for interstitial fibrosis. Mol Cell Biochem 1995; 147:29-34.

[115] Sandgaard NCF, Andersen JL, Holstein-Rathlou NN, Bie P. Aortic blood flow subtraction: an alternative method for measuring total renal blood flow in conscious dogs. Am J Physiol Regul Integr Comp Physiol 2002; 282:R1528-R1535.

[116] Sarin SK, Sabba C, Groszmann RJ. Splanchnic and systemic hemodynamics in mice using a radioactive microsphere technique. Am J Physiol Gastrointest Liver Physiol 1990; 258:G365-G369.

[117] Schaper W, Winkler B. Of mice and men – the future of cardiovascular research in the molecular era. Cardiovascular Research 1998; 39:3–7.

[118] Schneider JE, Cassidy PJ, Lygate C, Tyler DJ, Wiesmann F, Grieve SM, Hulbert K, Clarke K, Neubauer S. Fast, High- Resolution In Vivo Cine Magnetic Resonance Imaging in Normal and Failing Mouse Hearts on a Vertical 11.7 T System. Journal of Magnetic Resonance Imaging 2003; 18:691-701.

[119] Schneider JE, Hulbert KJ, Lygate CA, Hove MT, Cassidy PJ, Clarke K, Neubauer S. Long-term stability of cardiac function in normal and chronically failing mouse hearts in a vertical-bore MR system. MAGMA 2004; 17: 162–169.

[120] Schneider JE, Lanz T, Barnes H, Lee-Anne Stork, Bohl S, Lygate CA, Ordidge RJ, Neubauer S. Accelerated cardiac magnetic resonance imaging in the mouse using an eight-channel array at 9.4 Tesla. Magn Reson in Med 2010; 65(1):60-70.

[121] Schwartz LA, Zuurbier CJ, Ince C. Mechanical ventilation of mice. Basic Res Cardiol 2000; 95:510-520.

[122] Shapiro EP. Evaluation of left ventricular hypertrophy by magnetic resonance imaging. Am J Card Imaging 1994; 8:310-315.

[123] Sharief A, Badea A, Dale AM, Johnson GA. Automated segmentation of the actively stained mouse brain using multi-spectral MR microscopy. Neuroimage 2008; 39:136–45.

[124] Sheuer J, Bahn AK. Cardiac contractile proteins: adenosine triphosphatase activity and physiological function. Circ Res 1979; 45:1-12.

[125] Siri FM, Jelicks LA, Leinwand LA, Gardin JM. Gated magnetic resonance imaging of normal and hypertrophied murine hearts. Am J Physiology Am. J. Physiol. Heart Circ. Physiol. 1997; 272(41): H2394-H2402.

[126] Slawson SE, Roman BB, Williams DS, Koretsky AP. Cardiac MRI of the normal and hypertrophied mouse heart. Magnetic Reson in Med 1998; 39:980-987.

[127] Smaill B, Hunter P. Structure and function of the diastolic heart: Material properties of passive myocardium. In Glass L, Hunter P, McCulloch A, Theory of heart: biomechanics, biophysics, and nonlinear dynamics of cardiac function. Chapter 1: Springer-Verlag; 1991. p 1-29.

[128] Sosnovick DE, Dai G, Nahrendorf M, Rosen BR, Seethamraju R. Cardiac MRI in mice at 9.4 Tesla with a transmit-Receive surface coil and a cardiac-tailored intensity-correction algorithm. J. Magn Reson Imaging 2007; 26:27-287.

[129] Staehle F, Jung BA, Bauer S, Leupold J, Bock J, Lorenz R, Foll D, Markl M. Three-Directional acceleration phase mapping of myocardial function. Magn Reson in Med 2011; 65:1335-1345.

[130] Streif JUG, Herold V, Szimtenings M, Lanz TE, Nahrendorf M, Wiesmann F, Rommel E, Haase A. In Vivo Time-Resolved Quantitative Motion Mapping of the Murine Myocardium With Phase Contrast MRI. Magnetic Resonance in Medicine 2003; 49:315–321.

[131] Streif JU, Nahrendorf M, Hiller KH, Waller C, Wiesmann F, Rommel E, Haase A, Bauer WR. In vivo assessment of absolute perfusion and intracapillary blood volume in the murine myocardium by spin labeling magnetic resonance imaging. Magn Reson in Med 2005; 53(3):584-592.

[132] Stoker ME, Gerdes AM, May JF. Regional differences in capillary density and myocyte size in the normal human heart. Anato Rec 1982; 202(2):187-191.

[133] Stuckey DJ, Carr CA, Martin-Rendon E, Tyler DJ, Wilmott C, Cassidy PJ, Hale SMJ, Schneider JE, Tatton L, Harding SE, Radda GK, Clarke K. Iron particles for non-invasive monitoring of bone marrow stromal cell engraftment and isolation of viable engrafted donor cells from the heart. Stem Cells 2006; 24: 1986-75.

[134] Stuckey DJ, Carr CA, Camelliti P, Tyler DJ, Davies KE, Clarke K. In vivo MRI characterization of progressive cardiac dysfunction in the mdx mouse model of muscular dystrophy. PLoS ONE 2012; 7(1):e28569.

[135] Stull LB, Leppo MK, Marban E, Janssen PM. Physiological determinants of contractile force generation and calcium handling in mouse myocardium. J Mol Cel Cardiol 2002; 34(10):1367-76.

[136] Stuyvers BDMY, Miura M, Ter Keuers HEDJ. Dynamics of viscoelastic properties of rat cardiac sarcomeres during the diastolic interval: involvement of Ca^{2+}. J. Physiol Lond 1997; 502:661-677.

[137] Thireau J, Zhang BL, Poisson D, Babuty D. Heart rate variability in mice: a theoretical and practical guide. Exp. Physiol 2008; 93(1): 83-94.

[138] van Rugge P, van der Wall EE, Bruschke AVG. New Developments in Pharmacologic Stress Imaging. Progress in Cardiology 1992; 124(2):468-484.

[139] Webb S, Brown NA, Anderson RH. The structure of the mouse heart in late fetal stages. Anat Embryol Berl 1996; 194:37-47.

[140] Wiesmann F, Ruff J, Haase A. High-resolution MR imaging in mice. MAGMA 1998; 6:186-188.

[141] Wiesmann F, Ruff J, Dienesch C, Leupold A, Rommel E, Haase A, Neubauer S. Cardiovascular phenotype characterization in mice by high resolution magnetic resonance imaging. MAGMA 2000; 11(1-2):10-5.

[142] Wiesmann F, Neubauer S, Haase A, Hein L. Can we use vertical bore magnetic resonance scanners for murine cardiovascular phenotype characterization? Influence of upright body position on left ventricular hemodynamics in mice. J. Cardiovascular Magn Reson 2001; 3(4):311-315.

[143] Wiesmann F, Frydrychowicz A, Rautenberg J, Illinger R, Rommel E, Haase A, Neubauer S. Analysis of right ventricular function in healthy mice and a murine model of heart failure by in vivo MRI. Am J Physiol Heart Circ Physiol 2002; 283: H1065–H1071.

[144] Wiesmann F, Ruff J, Engelhardt S, Hein L, Dienesch C, Leupold A, Illinger R, Frydrychowicz A, Hiller KH, Rommel E, Haase A, Lohse MJ, Neubauer S. Dobutamine-Stress Magnetic Resonance Microimaging in mice: acute changes of cardiac geometry and function in normal and failing murine hearts. Circulation Research 2001; 88:563-569.

[145] Wilding JR, Schneider JE, Sang AE, Davies KE Neubauer S, Clarke K. Dystrophin- and MLP-deficient mouse hearts: marked differences in morphology and function, but similar accumulation of cytoskeletal proteins. FASEB J 2005; 19(1):79-81.

[146] Williams SP, Gerber HP, Giordano FJ, Peale FV, Bernstein LJ, Bunting S, Chien KR, Ferrara N, van Bruggen N. Dobutamine Stress Cine-MRI of Cardiac Function in the Hearts of Adult Cardiomyocyte-Specific VEGF Knockout Mice. J. Magnetic Resonance Imaging 2001; 14:374-382.

[147] Young A, Frangi AF. Computational cardiac atlases: from patient to population and back. Exp Physiol 2009; 94(5):578–96.

[148] Zamyadi M, Baghdadi L, Lerch JP, Bhattacharya S, Schneider JE, Henkelman RM, Sled JG. Mouse embryonic phenotyping by morphometric analysis of MR images. Physiol Genomics 2010; 42A:89-95.

[149] Zerhouni EA, Parish DM, Rogers WJ, Yang A, Shapiro EP. Human heart: tagging with MR Imaging – a method for noninvasive assessment of myocardial motion. Radiology 1988; 169(1):59-63.

[150] Zhang W, ten Hove M, Schneider JE, Stuckey DH, Sebag-Montefiore L, Bia BL, Radda GK, Davies KE, Neubauer S, Clarke K. Abnormal cardiac morphology, function and energy metabolism in the dystrophic mdx mouse: an MRI and MRS study. J. Mol Cell Cardiol 2008; 45(6):754-60.

[151] Zhou R, Pickup S, Glickson JD, Scott CH, Ferrari VA. Assessment of global and regional myocardial function in the mouse using cine and tagged MRI. Magn. Reson in Med 2003; 49(4):760-764.

[152] Zhong X, Spottinswoode BS, Meyer CH, Kramer CM, Epstein FH. Imaging three-dimensional myocardial mechanics using navigator-gated volumetric spiral cine DENSE MRI. Magn Reson in Med 2010; 64(4):1089-1097.

IntechOpen